RESEARCH ARTICLE

VOLCANICA

The Moinui Flow on Mauna Loa: transport and deposition of an olivine crystal cargo in a compound basaltic lava flow

Stephen J. Barnes*[α], Thorvaldur Thordarson[β], Robin E.T. Hill[α], Caroline S. Perring[α,γ], Sarah E. Dowling[α], and Belinda Godel[α]

[α] CSIRO Mineral Resources, Kensington, Perth, Australia.
[β] Faculty of Earth Sciences, University of Iceland, Reykjavik, Iceland.
[γ] Current address: BHP, Resource Centre of Excellence, Perth, Australia.

Submitted: 2023-12-04 | Accepted: 2024-04-09 | Published: 2024-05-13

Editor: K. Chamberlain | Typesetter: E. Maters

Abstract

The Moinui lava flow on the west flank of Mauna Loa, Hawai'i, is a 32-km-long pāhoehoe basalt flow, between 760 and 1500 years old, characterised by the presence of two generations of olivine: 2–5-mm-sized glomerocrystic clusters of equant polyhedral grains, and dendritic plates. Both generations are distributed throughout the flow field from the vent at 3400 m above sea level to the ocean. We mapped roadcut outcrops in detail to investigate the internal geometry and emplacement mechanisms of the flow, and sampled these outcrops to collect quantitative textural data on the two olivine populations in 2D and 3D, with a view to understanding emplacement processes in general, and the factors controlling the growth, transport, and deposition of phenocryst olivine in particular. Roadcut outcrops reveal complex geometries of interconnected tube-fed sheet lobes, with the main control being pre-existing topography: drained tubes with flanking sheet lobes were developed on the seaward slope of the volcano, whereas tumuli were developed on the flat coastal plain topography. The internal architecture of the flow field is consistent with current hypotheses of emplacement by breakout and inflation of flow lobes from tube-fed internal pathways. Concentrations of up to 30 % olivine are found primarily within thicker lobes and represent settling of the larger size-fraction of the transported load, with no evidence for superimposed effects of flow differentiation. Implied effective viscosities were around 1000 Pa s. The glomerocrystic population was inherited as pre-existing crystal clusters derived from a sub-volcanic chamber, rather than by synneusis (random collision and aggregation) post-eruption, whereas the plate population was probably generated by a burst of nucleation related to degassing and supercooling during the vent eruption. Other than this, there is no evidence for substantial growth of the transported olivines during flow.

Non-technical summary

Lavas are commonly erupted carrying cargos of crystals that formed somewhere in the plumbing system beneath the volcano, and these crystal cargos can give useful information about the passage of magma to the surface. The Moinui lava flow on Mauna Loa, Hawai'i, is one such example. The lava contains two populations of olivine crystals: clusters of touching grains, and an unusual population of dendritic crystals that we have concluded formed during the eruption itself. Subsequent to eruption, lava flowed over 30 km to the sea in a series of interconnected lobes and tubes. The internal structure and geometry of the flow shows that it developed as a complex series of interconnected tube-fed inflating lobes, whose architecture depended mostly on the topography of the substrate. The distribution of the olivine populations in a set of samples collected along the flow path gives us clues as to how long this took, and what the internal processes were within the lava. Investigation of the geometry of the olivine clusters using 3D X-ray microtomography provides some important new insights. The nature of the olivine clusters has broader relevance to an ongoing debate among igneous petrologists about how crystals nucleate and grow from magmas.

Keywords: Basalt; Hawai'i; Inflation; Pahoehoe; Settling; Synneusis; Nucleation; Dendrites; Glomerocrysts; Aggregating.

1 Introduction

Populations of transported crystal cargoes in lava flows are widely used as indicators of subvolcanic processes, potentially recording pre-eruption magma evolution and residence times in sub-volcanic storage zones and conduits and providing information about magma mixing processes and sub-surface transport mechanisms [Costa and Dungan 2005; Ganne et al. 2018; Ubide and Kamber 2018]. However, it is likely that some modification of crystal loads takes place during eruption through crystal growth, and during mechanical crystal-liquid separation through processes such as gravitational settling and flow differentiation [Rowland and Walker 1988]. Hence, mechanisms of concentration of olivine within lava flows have potential application to the origins of cumulate rocks in general. Since olivine cumulates are commonly associated with economic concentrations of Ni-Cu-rich magmatic sulfides in sill-dyke complexes and in komatiite lava flows [Barnes et al. 2016; Gole and Barnes 2020], enhanced understanding of their formation may have economic value as well.

The pre-historic picritic Moinui lava flow field on Mauna Loa (Hawai'i, USA) is typified by two distinct populations of olivine macrocrysts: a glomeroporphyritic crystal-cluster population carried by the magma from depth and a dendritic platy-shaped population formed during conduit transit and/or lava emplacement [Perring et al. 2004; Couperthwaite et al. 2020]. This provides insight into the processes of growth, transport, and deposition of both types of macrocrysts and allows these aspects of their history to be placed into a physical

* steve.barnes@csiro.au

volcanological context. The dendritic population is of particular interest, given recent suggestions that early dendritic growth of olivine may be a much more widespread process than previously recognised [Welsch et al. 2013]. Furthermore, glomerocrystic crystal clusters are relevant to a current debate as to whether crystal clusters form by accidental collisions and adhesion (synneusis) [Schwindinger and Anderson 1989; Holness et al. 2017; Wieser et al. 2019], by the process suggested by Campbell [1978] of heterogeneous self-nucleation, or by entrainment and disaggregation of pre-existing sub-volcanic cumulates [Dowty 1980; McIntire et al. 2019]. This distinction is important for current discussions on crystal nucleation and growth mechanisms in magma chambers and the origins of some orthomagmatic ore deposits such as chromite seams [Holness et al. 2022; Latypov et al. 2022] with implications for the existence or otherwise of large magma chambers in the crust [Latypov et al. 2022].

We have quantitative petrographic data on a large suite of samples representative of the very proximal to the distal sectors of the Moinui lava flow field, the range of lava types that typify the flow field and the spatial variations of the olivine populations within individual cooling units. This sample set provides an opportunity to ask a number of questions regarding flow emplacement processes and mechanisms of growth, sorting, and accumulation of phenocrysts. Specifically:

1) Is the internal architecture of the flow field consistent with current hypotheses of emplacement by breakout and inflation of flow lobes from tube-fed distributory pathways? What factors (e.g. proximity to vent, pre-existing substrate topography) control this architecture?

2) What is the origin and relative timing of formation of the two olivine populations? Particularly, are the glomerocrysts the result of post-eruption synneusis?

3) Are olivine phenocrysts physically concentrated and/or modified by processes of gravitational settling and/or flow differentiation within the distributory pathways?

4) Can the extent of settling be used to derive estimates of time-scales of lava emplacement and effective lava viscosity?

To these ends, we investigated the 3D internal architecture of the basaltic flow field and crystal transport and deposition mechanisms at multiple points along the length and width of the flow. We compare samples from vent to distal position, emplaced on steep slopes and on the flat coastal plain, relating detailed quantitative textural data on olivine to sample location with respect to lobe and tube geometry.

A brief note on terminology is needed: “glomerophyric” is a textural term referring to a rock and denotes the presence of phenocrysts as connected clusters or aggregates of grains (we use the term cluster from here on for brevity). “Glomerocrystic” describes individual crystals within the clusters and describes the clusters themselves. “Platy” refers to plate-shaped dendritic crystals. “Pathways” refers to parts of the flow that served as feeders to flanking lobes; pathways are commonly marked by evidence of former tube-constrained flow; “sheet lobes” refers to planar cooling units with flat aspect ratios lacking evidence of internal pathways.

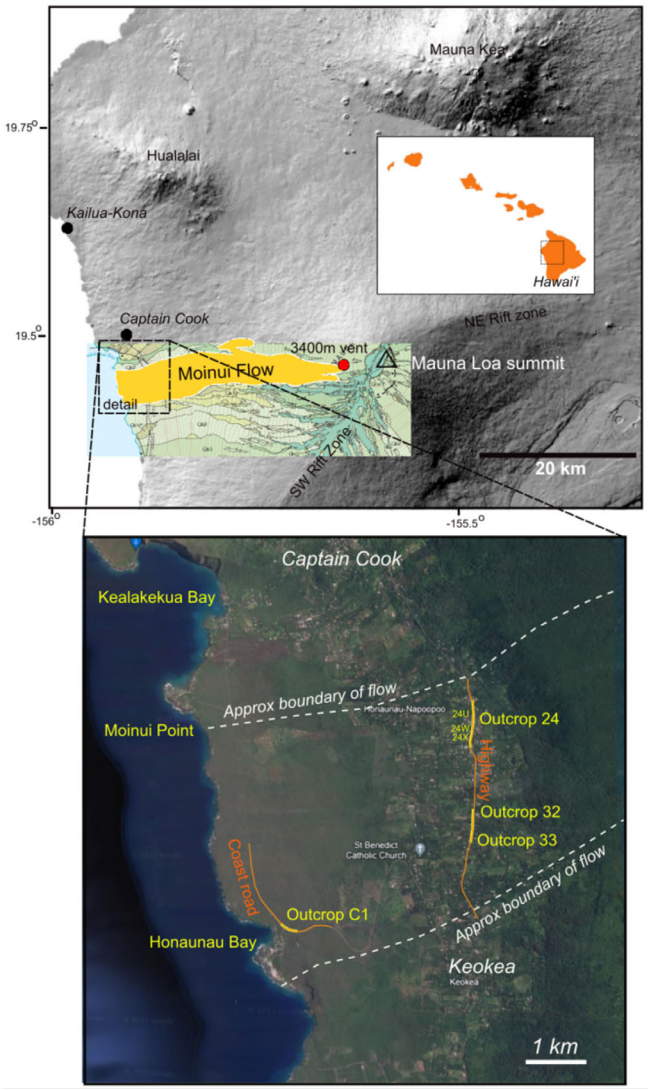

Figure 1: Location. [Top] Digital elevation map of western part of island of Hawai‘i (source: https://gis.ess.washington.edu/data/raster/tenmeter/hawaii/), showing outline of the Moinui Flow from the USGS Geological Map of Hawai‘i [Sherrod et al. 2021] and position of the 3400 m vent. [Bottom] Detailed Google Earth image of study area showing location of the sampled roadcuts.

2 Geological setting

2.1 Mauna Loa - setting and activity

Mauna Loa rises ~9 km above the floor of the central Pacific (4167 m above sea level) and is the largest volcano on Earth. The summit crater Moku‘aweoweo forms an elongate 15 km^2 caldera and linked to two rift zones extending to the east-northeast (NERZ) and to the southwest (SWRZ) (Figure 1). Since 1832, when the first recorded “historical” eruption occurred [Barnard 1995], 39 eruptions have been documented and their lava flow fields have covered over 800 km^2 of the volcano’s flanks, where each event has emplaced 0.25–0.5 km^3 of lava in a few days to weeks. From 1843 to the present, individual events have begun with activity near or at the summit

crater and a few days later more voluminous flank eruptions have followed [Lockwood and Lipman 1987]. The origin of pre-1843 eruptions such as Moinui is less well-known due to the burial of older flows by younger lavas and due to deep weathering [Trusdell and Lockwood 2017].

The 750–1500-year-old Moinui lava flow field (Figure 1) originated from vents on the upper slopes of the SWRZ, just west of Mauna Loa's summit at ~3400 m above sea level [e.g. Trusdell and Lockwood 2017], forming part of the QK3 member of the Kaʻu basalt according to the 2021 USGS Geological Map of Hawai'i [Sherrod et al. 2021]. It is 32 km long, extending westwards to the coast between Palemano Point on the south side of Kealakekua Bay and Pu'uhonua Point on the south side of Honanau Bay, and takes its name from the westernmost subaerial extension of the flow field, Moinui Point [e.g. Trusdell and Lockwood 2017]. It is very well exposed in road cuts along the coast road near the entrance to Puʻuhonua o Honaunau State Park and along Highway 11 just north of Keokea (Figure 1).

Moinui is a pāhoehoe flow field [Walker 1971] with unweathered exposure of lava in a series of well-exposed roadcut outcrops available for logging and sampling. Samples were collected in relation to detailed mapping from outcrop C1 on the coast road and outcrops 24, 32, and 33 on the highway (Figure 1). Samples were also collected from a site at or very close to the original eruption vent at ~3400 m of elevation on the upper flank of Mauna Loa. Perring et al. [2004] and Couperthwaite et al. [2020] showed that the Moinui lava is typified by two morphologically distinct types of olivine phenocrysts, of which one is in the form of clusters of polyhedral grains (glomerocrysts) and the other is platy (Figure 2). Couperthwaite et al. [2020] show that the glomerocrysts have core compositions of $Fo_{90–88}$ far out of equilibrium with the transporting lava, while the rims are typically in the $Fo_{82\text{-}84}$ range and in near equilibrium with the observed erupted melt composition. The fosterite content in the platy olivine cores ($Fo_{83–82}$) is similar to that of the rims on the glomerocryst olivines, while platy rims have the lowest Fo-content ranging from $Fo_{78\text{-}65}$. Couperthwaite et al. [2020] also combined field, textural and geochemical data with microprobe analysis of diffusion profiles in the glomerocrystic and platy olivine to assess timescales of crustal transport and storage: months to years in the case of the glomerocryst, days for the platy grains.

3 Field observations and sampling

The objective of the outcrop field observations was twofold: (i) to document the internal architecture of a large-scale tube-fed pāhoehoe flow field and (ii) to investigate the distributions, morphologies, and grainsizes of olivine macrocryst populations in 2D and vertical profile, in relation to (i).

The flow field architecture was obtained via detailed cross-sectional mapping of each outcrop at a scale of about 1:10, documenting in each outcrop the lobe types, their form and dimensions along with taking notes on the arrangement of internal structure, such as lower crust, lava core, and upper crust, and flow rubble when present. Composites of lobe arrangements were made using outcrop photo mosaics (see Supplementary Material), then perspective-warped in Photoshop™ to correct for the non-vertical profile of most of the outcrops such that the maps represent projections onto vertical surfaces parallel to the outcrop. Samples were collected by hammer directly from the outcrop surface with orientations noted where necessary. In the case of the 3400-m-elevation vent samples, these were collected during a single helicopter-supported sampling trip such that detailed lobe mapping was not possible.

4 Methods

Thin sections were cut for almost all the samples collected. Quantitative image data was obtained from ~150 samples. Digital photo mosaics of complete thin sections were processed using the image processing procedure of Perring et al. [2004], and subsequently segmented into three components: olivine, vesicles, and groundmass (glassy or microcrystalline). Olivine grains were then sub-divided into polyhedral and platy categories by manually colouring the glomerocryst olivines in each sample using the paint bucket tool in Photoshop™, which applies a colour to contiguous pixels. Touching vesicles were separated into component subcircular (in cross-section) individual objects using a watershed algorithm. The segmented images were then measured using the image processing function in the software package Aphelion to yield modes and size characteristics of vesicles and olivine. Where platy olivines were measured in samples with shape preferred orientation (usually a lamination) the section was cut orthogonal to the plane of the lamination. Given the dendritic and skeletal nature of many platy olivine grains it is unlikely that the correction fully retrieves the original volume of the crystal. Hence, these measurements can only be used for comparison between samples and are not applicable for estimation of residence times or growth rates. Because of the highly connected geometry of the glomerocrystic clusters, we abandoned an early attempt to separate the individual crystals via the watershed segmentation; the crystal size data reported is, therefore, derived from the 2D area of the cluster and represents the volume of the entire cluster, not the individual crystals within it. This is a further reason why the grain size data should not be used for quantitative estimates of nucleation rates and residence times. All olivine mode measurements are presented vesicle-corrected, i.e. % mode in thin section × 100/[100 − % vesicle mode].

The image processing dataset allows for a wide variety of different measurements of apparent grain size, of which the most comprehensible is the size of the minimum bounding rectangle, that is the smallest rectangle which can be drawn to completely enclose the grain in 2D. However, this does not take account of the "openness" of the crystal clusters, which varies widely, and a single projecting elongate grain can make a small cluster appear much bigger. Hence the method used here is to calculate an "equivalent circle diameter", or ECD, which is the diameter of the circle having the same area as the measured 2D area of the grain in 2D in thin section (also known as the Heywood diameter).

Many thousands of measurements of segmented vesicle sizes were collected but interpretation of this dataset is be-

yond the scope of this paper. Data are available from the CSIRO digital access portal*.

Methods for whole rock geochemical analysis and microprobe analysis of olivine are reported by Couperthwaite et al. [2020]. The synchroton XFM images shown in Figure 2 were collected on the XFM beamline at the Australian Synchroton [Ryan et al. 2014] at an input beam energy of 17.5 keV and a raster resolution of 4 µm. These provide high spatial resolution (~2 µm) images showing details of groundmass textures and chemical zoning of grains. X-ray microtomography images were collected and processed following the procedures described by Godel [2013] using a Zeiss Versa XRM 520 3D X-ray microscope at the Australian Resources Research Centre (Kensington, Western Australia).

5 Petrography

Sample-scale petrography within the Moinui lava is highly variable, even on the scale of individual lobes. The range in vesicularity is from ≤1 % up to 50 %. Modal abundance of olivine macrocrysts ranges from <1 % to >30 %, corrected for vesicularity. The groundmass crystallinity varies from hypohyaline at quenched lobe margins to holocrystalline with plagioclase-clinopyroxene-Ti-magnetite intergrowths, while in size terms it ranges from crypto- to microcrystalline.

The photomicrographs and synchrotron XFM images in Figure 2 and Figure 3 clearly show the distinct olivine generations: the polyhedral olivine macrocrysts, commonly glomerocrystic, consisting of clusters of up to ~15 olivine grains (in 2D) in face and point contact, with individual grain diameters typically ~2 mm; and the dendritic platy olivines, whose complex geometry is visible in the grain in Figure 2C and D where the grain is intersected face-on. Henceforth we refer to these two generations as glomerocrysts (or glomerocrystic clusters) and plates.

As shown by Couperthwaite et al. [2020], the glomerocrystic clusters have distinct, sharply defined outer zones of Fe enrichment. These outer rims have similar compositions to the platy olivines (although some of these also have lower Fe cores, as in the dendritic grain in Figure 2C and D). The Fe-rich outer rims are developed around the margins of the clusters, rather than around the individual component grains, indicating growth of the rims postdated aggregation. Some of the larger dendritic plates also have Mg-rich cores (e.g. Figure 2D) indicating that dendritic growth took off from a pre-existing entrained nucleus.

An incidental observation from one of the synchrotron maps is that a patch of groundmass sitting in a vesicle (Figure 2C, E), enriched in Ti and other incompatible components, is segregated melt produced by gas filter pressing of residual fractionated groundmass melt into the edge of a vesicle and thus is a segregation vesicle [Smith 1967; Anderson et al. 1984]. These types of vesicles are common in the basal and upper crust of lava lobes [Thordarson and Self 1998], and have also been identified in shallow intrusions [Barnes and Robertson 2019].

The vent-proximal samples (3400 m vent site) are generally similar to those from the distal highway and coast road sites. In Figure 3 the platy component appears to be somewhat less abundant and finer grained, as discussed quantitatively below, but this may be an artifact of a relatively restricted number of samples.

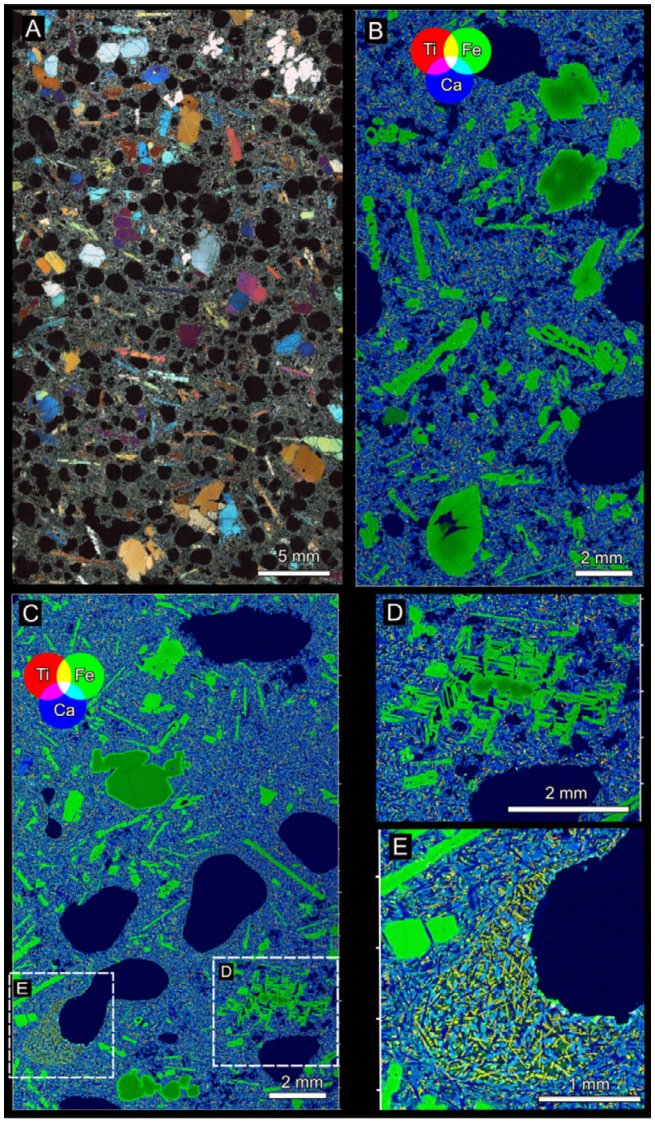

Figure 2: Petrography of Moinui Flow samples (from C1 coast road tumulus outcrop) with microcrystalline ground mass and two distinct olivine morphologies, overview. [A] Photomicrograph mosaic, whole thin section, ~6 cm across. [B, C] False colour RGB microbeam XRF maps (resolution 8 µm pixels). Note distinct high-Fe outer zones (lighter green) on olivines; distinct touching-sphere geometry of vesicles in [A] compared with coarser lobate partially coalesced vesicles in [B]; strongly dendritic nature of olivine plate in [B] (lower left seen face-on, enlarged in [D]) with a central Mg-rich core, and presence of a Ti-enriched segregation vesicle in lower left of [B], enlarged in [E]; highly irregular diktytaxitic porosity (black) in [C], due to volume contraction during groundmass solidification.

*https://data.csiro.au/collection/csiro:61210

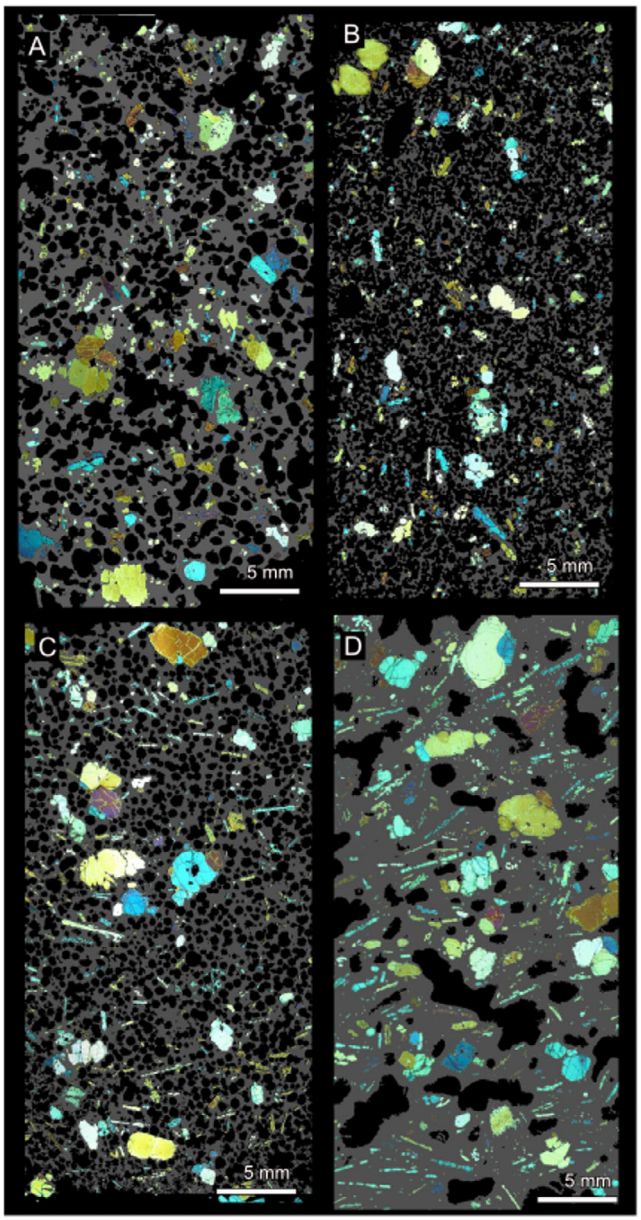

Figure 3: [A, B] Processed images of samples from the 3400 m vent locality and [C, D] highway outcrops. Olivine mask (maximum birefringence images as described by Perring et al. [2004]) over segmented vesicles (black) and groundmass (grey). Note general similarity in phenocryst olivine populations over 30 km length of flow. [A] Partially coalesced vesicles, lower plate content; [B] heterogeneous spongy and vesicle poor glassy sample; [C] spongy fine vesicles from lobe crust, aligned plates; [D] coarse coalesced vesicles in lobe core, aligned plates.

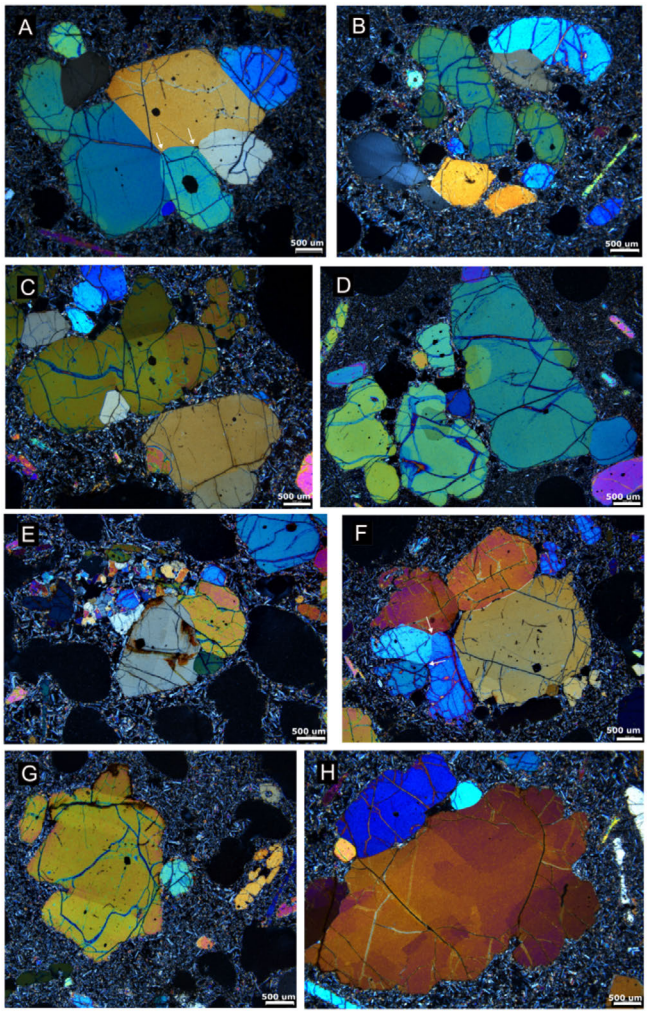

Figure 4: Detailed features of glomerophyric olivine clusters in 2D. Transmitted light, crossed polars. All samples from outcrop 24. [A] Close-packed cluster, grains in full face contact showing smooth grain boundaries, annealed 120-degree triple grain boundaries (arrowed). [B] More typical loose-packed cluster, most grains in point or limited face contact. [C, D] Typical mixture of point and face contacts, note presence of smaller euhedral faceted grains partially or entirely enclosed in larger ones. Central grain in [C] shows internal sub-grain development. [E] Composite cluster also including plagioclase-olivine-cpx intergrowth. [F] Compact cluster with annealed grain boundaries, intermediate between [A] and [B]. [G] Coarse grain showing lamellar subgrains possibly due to lattice strain. [H] Compact cluster, large grain showing complex assemblage of irregular internal subgrains.

5.1 Detailed petrography of olivine clusters

Higher-resolution images of individual olivine clusters are shown in Figure 4. Bearing in mind uncertainty due to sectioning effects, there appears to be a spectrum from relatively close-packed, compact clusters with most grains in face contact (Figure 4A) to more open chains or cages with grains showing either point contact or contact along a small proportion of the length of the impinging faces (Figure 4B), with most falling somewhere between. Face contacts are commonly smooth but curved, implying grain growth to impingement. Across this spectrum, a common feature in most clusters is the presence of small partially or completely enclosed, typically euhedral faceted grains fully enclosed in larger grains (Figure 4C, D).

A significant feature of interest is the common presence of internal subgrains with low-angle misorientations in some

(probably ~5–10 %) of the larger grains (Figure 4H). In most cases, these misorientation boundaries appear to be low-angle face contacts between adjacent homogeneous grains with very similar orientations (Figure 4C) but in others (Figure 4G) they appear to be deformation microstructures, presumably predating the incorporation of the grain into the cluster. A small proportion (less than 1 %) of clusters are polymineralic (Figure 4E) containing clinopyroxene and plagioclase in between the olivine grains, with distinctly coarser grain size than the basalt matrix. A few clusters of plagioclase grains were also observed, in less than 5 % of samples.

5.2 3D imaging

Three samples were investigated using X-ray computed tomography (CT), one using relatively low resolution with a medical scanner (Figure 5) and the second (Figure 6 and Figure 7) using the Zeiss high-resolution scanner, both at CSIRO. The high-resolution images show the marked contrast in morphology between the two generations of olivine. The high-resolution image in Figure 7 indicate the 3D geometry and extent of the polyhedral olivine clusters. Individual crystals are typically roughly equant to slightly elongate in overall geometry. Typically the clusters contain around 5–10 large grains (in 3D) and many smaller ones as encrustations on the surfaces. The geometry of the clusters is most clearly seen in the animated rotating 3D surface images available online*; an animation of a moving slice through the grey-scale image can also be viewed online†.

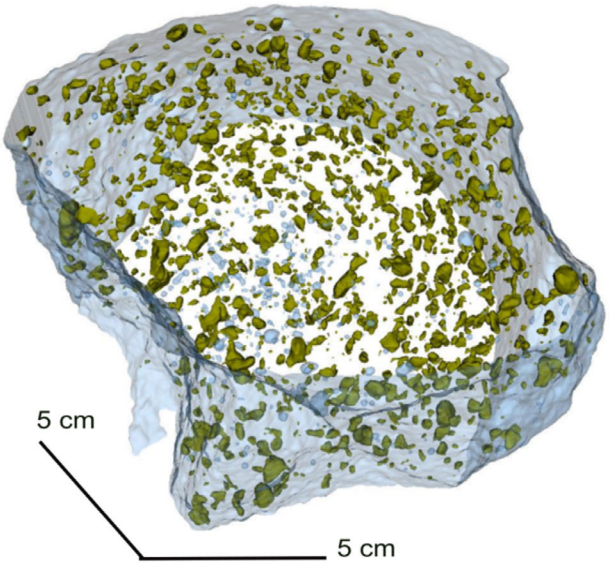

Figure 5: Low-resolution medical CT image (approximately 200 µm voxels) of a hand sample from the C1 coast road locality, showing glomerocrystic clusters of polyhedral olivine (in green) and some of the larger vesicles (blue). Plates are not visible in this image due to the low resolution.

*https://youtu.be/8Zo8q6gq3Ow
†https://www.youtube.com/watch?v=-qSWvAsnC8o

5.3 Olivine compositions

Olivines from throughout the flow field range from Fo_{90} in cores of glomerocrysts to Fo_{65} in rims [Couperthwaite et al. 2020], with a peak in rim compositions at around $Fo_{82.5}$ (Figure 8). The upper limit of the rim composition of the polyhedral olivine coincides almost exactly with the peak Fo content in plates. This is consistent with the notion that the rims of the polyhedral olivine equilibrated with the same melt that the plates grew from, whereas the cores are significantly out of equilibrium with the transporting magma as is commonly observed in basaltic lava flows [Ganne et al. 2018]. Olivines from the 3400 m vent samples (newly collected as part of this study) show an identical span in Fo content but are relatively deficient in crystals with high Fo cores (Figure 8).

Zoning of the glomerocrystic olivine clusters is evident in the XRF maps shown in Figure 2 and also (at somewhat lower resolution) in the high-resolution MicroCT images (Figure 6). Zoning patterns through the clusters are best revealed in the moving slice animations‡. In most cases, as noted above, the Fe-rich rim surrounds the entire cluster, rather than the individual grains. Based on close inspection of the moving slice image in the video associated with Figure 6, ~85 % of olivine-olivine grain pairs have mutual contacts between Mg-rich cores, with the remainder having contacts only between Fe-rich rims. This is an important observation in relation to testing the synneusis hypothesis, as discussed below.

6 Internal structure of the flow

The Moinui Flow is a pāhoehoe flow comprised of many thousands of individual flow lobes emplaced via endogeneous processes and lobe inflation [Walker 1971] separated by cooling surfaces. Minor ʻaʻā intercalations are present in some roadcut outcrops.

6.1 Highway traverse

The roadcuts along the Highway 1 island ring road (Figure 1, referred to from here on as the Highway outcrops) expose most of the width of the flow, in a location where it was emplaced on the sloping west flank of Mauna Loa. These outcrops expose a diverse array of individual flow lobes ranging from a few cm to 2 m in thickness, with highly variable width-to-height ratios. The smaller lobes can clearly be identified as lateral breakouts from individual tumuli, representing a nesting set of internal distributary pathways within the flow. Pāhoehoe and ʻaʻā lobes are both present, sometimes in the same roadcut (Figure 8), identifiable as being part of the same eruptive event by the presence of the same distinctive bimodal olivine population. ʻAʻā lobes are always subordinate, decreasing in abundance towards the centre of the flow along the Highway traverse, where the structure is dominated by stacked wide, flat pāhoehoe lobes and relatively low-aspect tumuli. Where ʻaʻā lobes are overlain by pāhoehoe, the pāhoehoe lobes tend to develop within the troughs between levees of ʻaʻā clinker (Figure 8). ʻAʻā is only present on relatively steeply sloping substrate. Some of the ʻaʻā is probably more accurately denoted as rubbly pāhoehoe [Keszthelyi et al. 2000].

‡https://youtu.be/mp5y4H6WZJ8

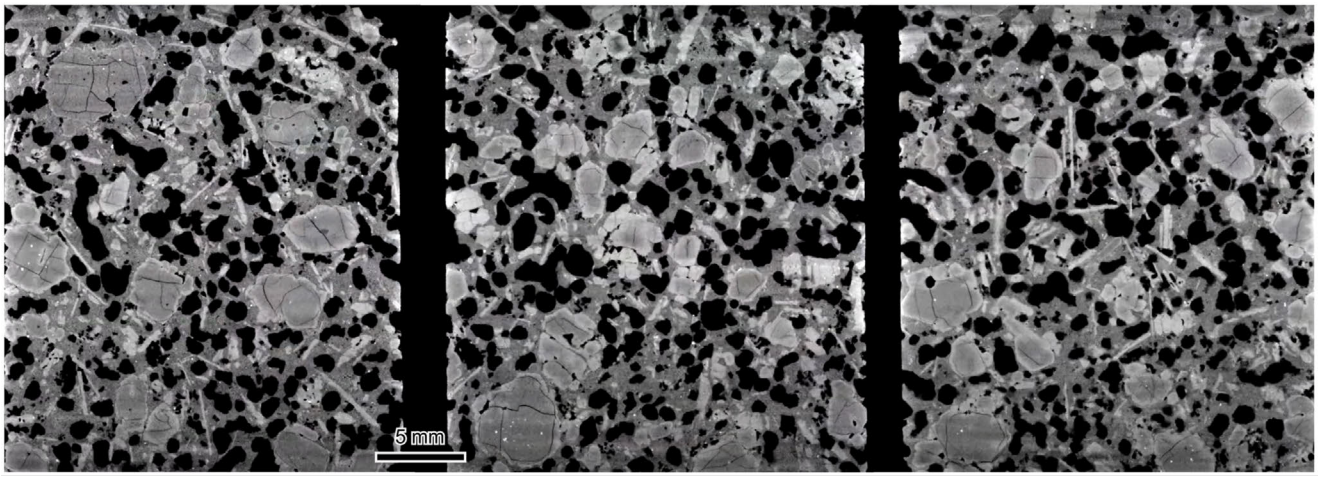

Figure 6: Successive slices ~5 mm apart through MicroCT image of an olivine-rich flow margin sample (outcrop 24, sample 24WM12) showing the two generations of olivine–glomerocrystic and platy (lighter grey)–and vesicles (black). Note the higher Fe content of the olivine rims and the plates indicated by the lighter grey shade. Note that plates are mostly seen side-on in this orientation and appear as needles. Small white grains inside olivine cores are chromite. An animation of sequential moving slices through this image can be seen at https://www.youtube.com/watch?v=-qSWvAsnC8o where the morphology of the platy grains is clear.

The lobes consist of an upper crust, a lava core (the central part of the lobe), and a basal crust [Self et al. 1997; Thordarson and Self 1998] where the upper crust and basal crust are distinguished on the basis of being more vesiculated than the dense interior or core [Aubele et al. 1988]. Vesicles tend to be coarser, less spherical, and more evidently coalesced within the cores, as seen by comparing Figure 3B (spongy margin) and 3D (core). Towards the upper and basal crust the vesicles become smaller and more spherical, forming spongy foam-like clusters as the groundmass grades from being microcrystalline in the core to glassy at the margins. Platy olivines tend to be strongly flow aligned within the glassy crusts and within 1–20 cm scale lava toes developed as apophyses on the lower crusts. Thin breakout lobes tend to be spongy and finely hypocrystalline throughout. These internal lobe structures are common features of pāhoehoe lobes, thus underpinning the notion that the Moinui Flow grew via processes of insulated lava transport and endogenous inflation [Self et al. 1996; Thordarson and Self 1996; 1998].

Lava tubes up to ~50 cm in height and 2 m wide are developed within many of these lobes (Figure 8). In some of these, a transition can be seen from heavy accumulation of coarse coalesced vesicles to gas-blisters, through cavities with flat floors showing incipient pāhoehoe surfaces, to fully developed drained tubes. In some cases, the tube or blister floors grade laterally from a clear cooling surface into a homogeneous lobe core (e.g. right-hand end of area B, Figure 8). ʻAʻā lobes take the form of lobe cores with microcrystalline groundmass entirely enveloped within a heavily-vesicular clinker crust.

From the lateral portions of the flow, exemplified by outcrop 24 (Figure 9), to the centre (outcrop 33, Figure 10), the proportion of ʻaʻā diminishes, the tumuli become broader and more planar, and the structure approaches a stack of interconnected sheet lobes with well-developed tubes. Smaller sheet lobes are clearly seen as lateral breakouts from distributary tubes and pathways.

The roadcut map for the C1 coast road outcrop (Figure 11) shows the changes related to emplacement of the lobes on the flat topography of the coastal bench within a few hundred metres of the current shoreline. Tumuli are broader and have more obviously hummocky topography, with a smaller proportion of decimeter-scale flanking breakouts. In addition, the coastal lobes typically contain pipe vesicles. Further up in the core they feature small vesicle cylinders containing vesicular segregation melt, features not seen in the Highway lobes that were erupted on steeper slopes.

6.2 Vertical lobe profiles

Four vertical profiles through selected lobes are shown in Figure 11 to Figure 14, showing distribution of different particle size fractions of olivine and vesicles. In all cases, particle sizes of clusters refer to the entire cluster, not the component crystals.

Two of these profiles show the expected gravitational concentration of olivine towards the base of the lobe, while one has the olivine peak within the lower crust, and the fourth has the peak at the top. All of the lobes shown here, and all of the thicker lobes mapped, show a consistent internal zonation from a glassy crust with abundant fine spherical vesicles, down through a zone of increasing vesicle size, to a central zone with a microcrystalline groundmass and typically less abundant but notably coarser and in some cases partially coalesced vesicles, down through a lower crust that typically mirrors the upper although generally thinner. Some lobes have developed cavities at the top of the pathways reflecting lowering of the level of the lava passing through with time. Others contain smaller flattened gas-blister cavities associated with very coarse coalesced vesicles.

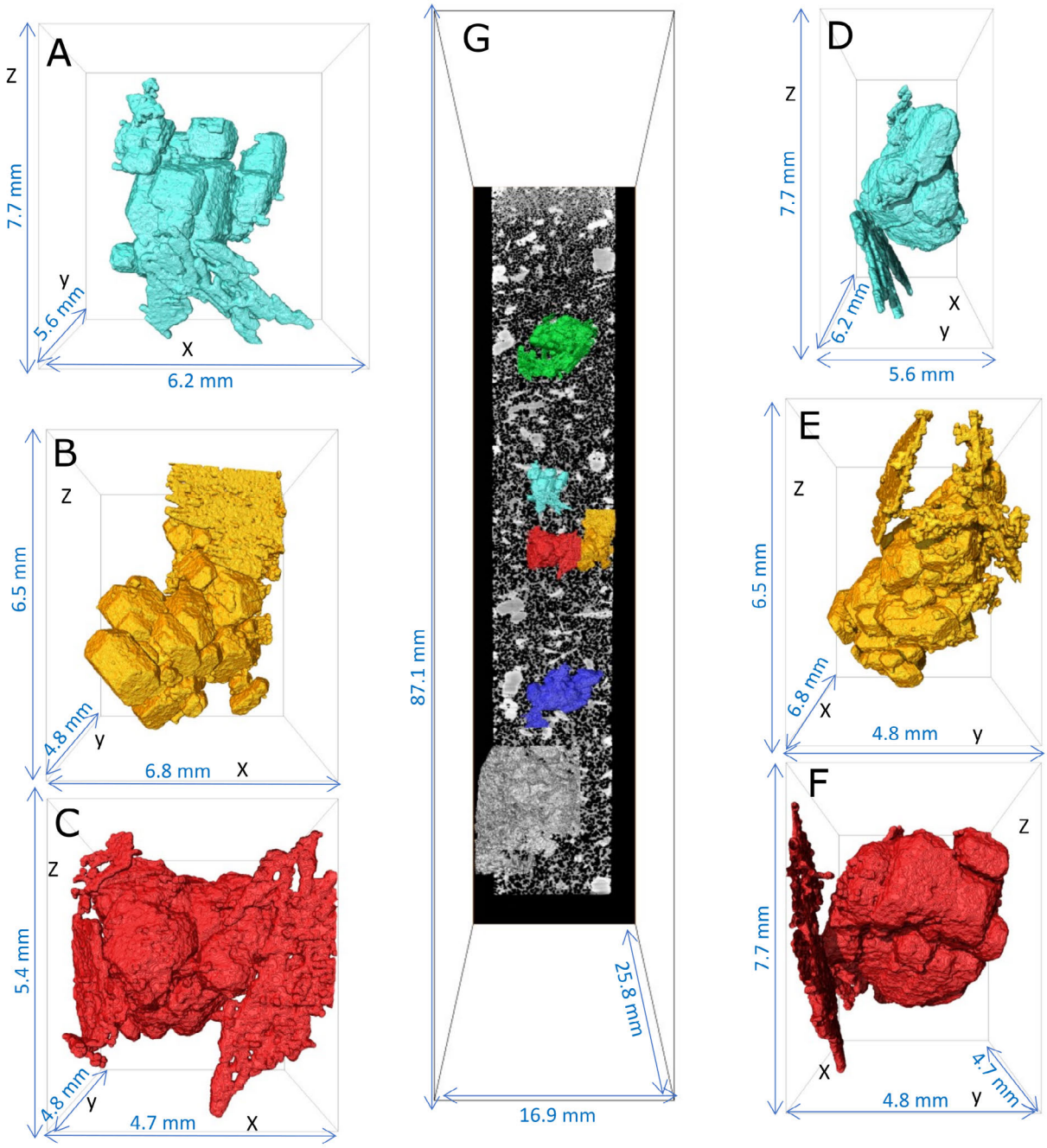

Figure 7: [A]–[F] MicroCT image of an olivine-rich flow margin sample (outcrop 24, sample 24WM12). 3D image of entire sample (centre) and surface renders of three individual olivine aggregates shown in two orthogonal orientations. Note predominant face contact of the idiomorphic grains, connection between plates and aggregates, and encrustation of large grain surfaces with small idiomorphic grains. Colours in central image [G] identify individual grain aggregates. Rotating animations of the surface renders of each of these aggregates are available at https://youtu.be/8Zo8q6gq3Ow and slice animations through each of the individual aggregates, showing Fe-Mg zoning as variations in greyscale, are available at https://youtu.be/mp5y4H6WZJ8.

6.2.1 *Outcrop 33B, lobe 5*

Lobe 5 in 33B (Figure 12) is a typical pāhoehoe sheet lobe with well-defined internal pathway and a large central cavity bound by vesicular basal (5–10 cm) and upper (45 cm) crusts. The peak olivine concentration is developed just below the cavity floor within a zone of coarse coalesced vesicles. The peak is mainly defined by olivine clusters greater than 2 mm in equivalent diameter, but there is also an increase in concentration of plates and smaller glomerocryst clusters at this level. Olivine polyhedral and platy crystal concentrations are similar in the top and bottom crusts. Also, the larger (>2 mm) olivine clusters are completely absent from the lobe above the peak position, indicating efficient settling during flow through the internal pathway. Vesicles are largely confined to the upper

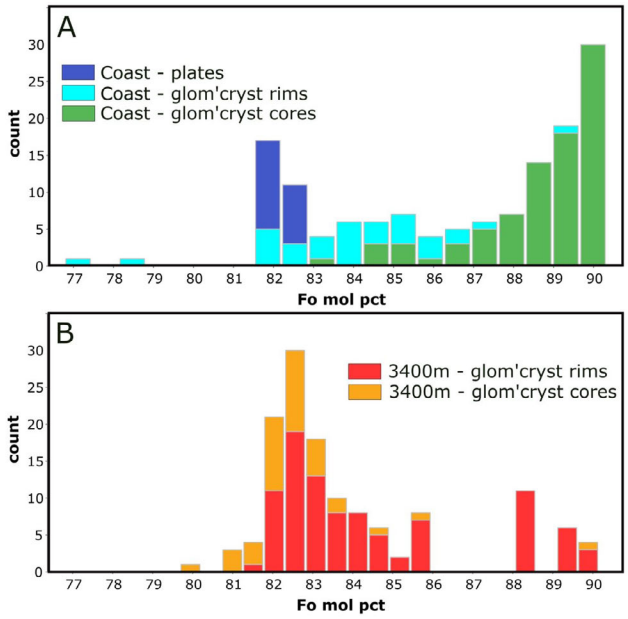

Figure 8: Olivine Fo contents measured in samples from 3400 m vent [A] and from within a tumulus on the C1 coast roadcut [B].

and basal crusts, although a distinct vesicle horizon is present around the void, interpreted as a consequence of the pressure drop associated with formation of a gas-blister. Maximum vesicularity is measured within the upper crust (30–50 %), which is typified by small (<1 mm in diameter) vesicles and a downward decreasing vesicle abundance (Figure 14A). A similar but reversed trend is observed in the basal crust, although the vesicle abundance is lower (15–25 %). By far the largest vesicles (>2 mm) are present in an approximately 15-cm-thick horizon at the base of the gas-blister, where they occur in abundance (>40 %), dropping off sharply downwards.

6.2.2 *Outcrop 24WM, lobe 4*

This is a pāhoehoe lobe, (Figure 13) ~120 cm thick in the sampled area, and at least 12 m long (the northern extent of the lobe is not exposed). There is large elongate void just above the lobe centre where the lobe is thickest. It represents the very top of an internal pathway and above it is the vesicular upper crust. As in lobe 33B, the lava below the floor of the void is highly vesicular, typified by large coalesced vesicles and features a pronounced zone of olivine concentration.

The abundance of platy olivine and <2 mm polyhedral olivine is rather uniform up through the lobe, which is different from lobe 33B-5 (see above) and almost all the variance in the olivine mode is taken up by the population of glomerocryst clusters that are >2 mm in minimum diameter (Figure 14B). The large clusters peak at ~30 % (vesicle corrected) at a depth of 80 cm below the lobe top and reach their minimum abundances immediately above and below the gas-blister.

Vesicles show a symmetrical sigmoidal distribution; the top and bottom of the lobe have just below 40 % fine spongy vesicles, the peak vesicularity of over 50 % is on either side of the gas-blister, and there is a strong minimum at ~20 % vesicle mode at ~90 cm below the lobe top, roughly corresponding to the olivine peak. The profile is clearly the result of flotation and coalescence of vesicles at the top of the free-surface that formed in the internal pathway when the flowing lava could not maintain contact with the base of the overlying roof. The pressure drop at the top of the moving lava associated with this separation resulted in concentration of large coalesced vesicles immediately below the floor of the drainage void and may, in part, explain the relatively low vesicle content in the lower part of the lava core. The abundance of fine vesicles increases abruptly and symmetrically towards top and bottom margins.

6.2.3 *Outcrop 24X, lobe 4*

This profile (Figure 14) shows some similarities with the last but differs significantly in that the maximum accumulation of olivine is right at the very base of the lobe, within a basal crust "toe" sample. This may represent an incipient early breakout from a parent tube, subsequently over-ridden by propagation of the main lobe. Again, only the glomerocryst size fraction >2 mm shows evidence for effective crystal settling, while the smaller glomerocrysts and plates are homogeneously distributed, with some tendency for plates to be more concentrated at the upper and lower margins. In this profile there is no clear upward concentration of vesicles within the core, and the interior of the lobe is generally less vesicular than the margins. It is likely that drainage of lava out from the tube resulted in a pressure drop within the liquid lava column, inducing vesiculation. Such vesicles can grow fast and hence rise towards the free surface or outgas into the void space formed by the partial tube drainage. Such features are widespread in the exposures along the Highway section (Figure 9, Figure 10).

6.2.4 *Outcrop 24WS, lobe 2*

The olivine distribution here (Figure 15) is completely different from the other two distributions, although the conclusion still holds that only glomero-clusters larger than 2 mm show significant modal variation. In this case, the highest olivine concentrations (and some of the highest seen anywhere so far) occur within a zone of coarse spongy spherical vesicularity just below the top surface. There is no apparent crystal settling trend in the lower part of the lobe. This crystal distribution clearly cannot be the result of simple in situ crystal settling and must imply a more complex mechanism, discussed further below.

7 Olivine distribution and particle size data

7.1 Size and shape distribution

The size and shape of olivine crystals and clusters is represented on a series of plots of aspect ratio–which is defined as the ratio of the lengths and width of the minimum bounding rectangle for each grain or cluster–against size, represented as equivalent circle diameter (Figure 16). Glomerocrysts and plates occupy distinctly different field in aspect versus size space, and this difference shows up in the proportion of glomerocrysts to plates in the different sampling regions (Figure 16A–C). We note that some plate measurements would appear more equant than they really are, on account of the orientation of the section; hence the wide range of aspect ratios for plates in Figure 16E. The 3400 m vent is

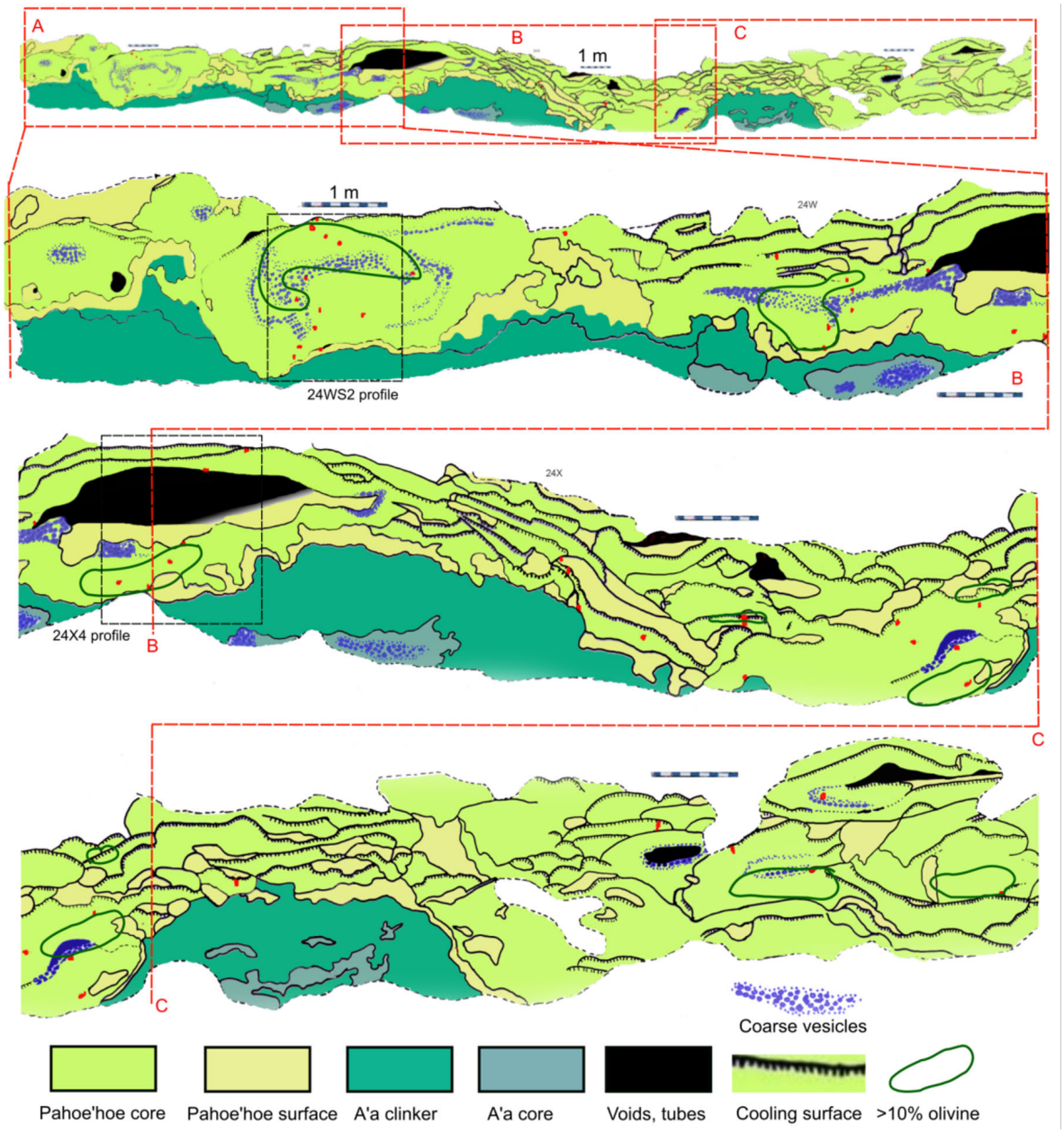

Figure 9: Map of Highway roadcut outcrop 24 (projected onto a vertical surface). See Figure 1 for location. This section, towards the northern margin of the flow, contains compound flow, pāhoehoe and ʻaʻā components, abundant large drainage cavities and proto-tubes, and one larger drained tube. Yellow colour indicates cooling surfaces dipping towards the road. Numbered red blobs are samples. Grey dots indicate concentrations of coarse coalesced vesicles within lobe cores. Dashed boxes indicate location of detailed profiles shown below.

dominated by generally smaller grains with a more limited range of aspect ratios (Figure 16A) compared with the overall plate population (Figure 16F); in other words, the plates are smaller and less distinctly developed in the near-vent samples, and the proportion of glomerocrysts is generally lower. This distribution can probably be taken as an indication of the crystal populations in the erupted lava at the vent, although caution must be applied given the great disparity in number of samples and the lack of available detail of the precise volcanic facies sampled. The (medial) Highway outcrops show a broad spread corresponding to a mix of both populations Figure 16B, while the (more distal) coast road samples are dominated by well-developed plates with a slightly smaller proportion of glomerocrysts (Figure 16C).

7.2 Overall modal variations

Modal proportions of platy and glomerocrystic olivine have been corrected for vesicle abundance and plotted in Figure 17 to compare modes for samples from the different sampling sites.

There is considerable variation in olivine distribution between different sites. Highway outcrops 24W and 24X. to-

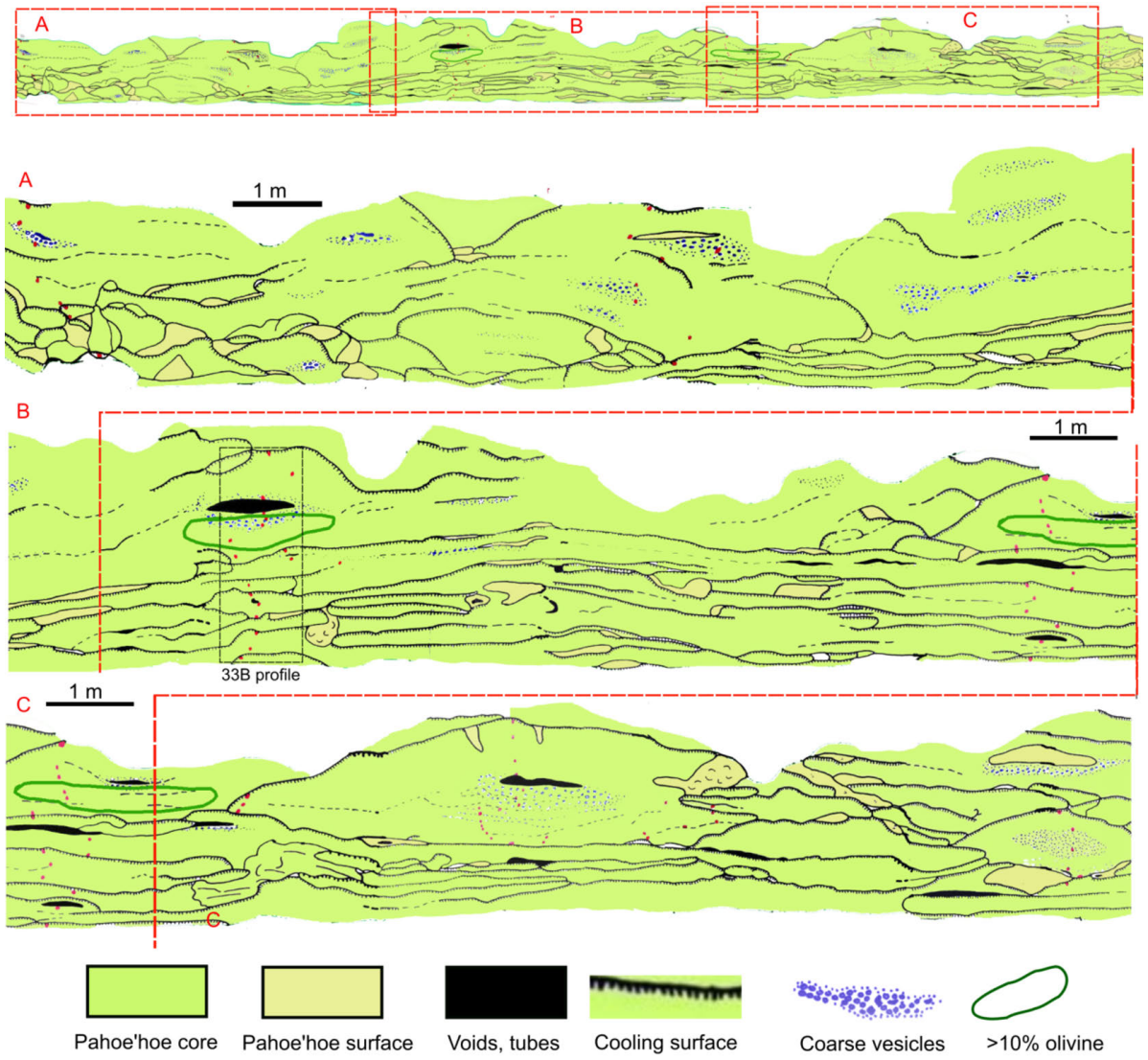

Figure 10: Outcrop 33, centre of flow field, Highway traverse (see Figure 1 for location). Note more laterally extensive sheet-like lobes and low-aspect tumuli with incipient lava tubes and an absence of ʻaʻā lobes.

wards the northern margin of the flow field, are very similar to one another in plate and glomerocryst abundances. The ʻaʻā lobes in outcrop 24U (to the north of 24X and W; see Figure 1) have similar olivine contents overall to 24W and 24XC but lack zones of glomerocryst olivine concentration. Samples from the 33B outcrop in the centre of the Highway traverse with rare exceptions are noticeably depleted in both plates and glomerocrysts compared to the 24 outcrops. Samples from the coast road Honaunau Bay outcrop C1 are also generally poor in plates and glomerocrysts but contain a few strongly olivine-rich samples. Samples from the 3400 m vent locality are distinctly poorer in the platy olivine component overall but overlap with the Highway outcrops in glomerocryst mode. There is no systematic correlation at all between blade and glomerocryst mode in any group apart from a weak positive correlation in outcrop 33.

Modal variation is a function of position in the lobe, as seen in Figure 18 (which is restricted to outcrops 24U, W and X where the most detailed roadcut mapping was carried out). Within both pāhoehoe and ʻaʻā flows there is less variation in olivine blade content than in glomerocryst content: most samples fall between 5 and 15 % plates, while glomerocrysts vary widely between 5 and 30 %. Most of this variation takes place within layered pāhoehoe lobes and can be found in both cores and crusts, although much of the variation in crusts is accounted for by four neighbouring samples from a single lobe, which may be anomalous. Excluding these samples, the bulk of the olivine variation in pāhoehoe lobes takes place within the layered cores and bottom crusts.

7.3 Particle size analysis

Crystal size distribution (CSD) plots [Cashman and Marsh 1988; Marsh 1988; 1998] describe populations of crystals in terms of the numbers of crystals within a certain size range per volume of rock. (In this study we imaged individual grains (dendrites) and glomerophyric clusters, so we use the term Particle Size rather than Crystal Size, hence PSDs). Image analyses of over 150 thin sections [Perring et al. 2004] gives us a

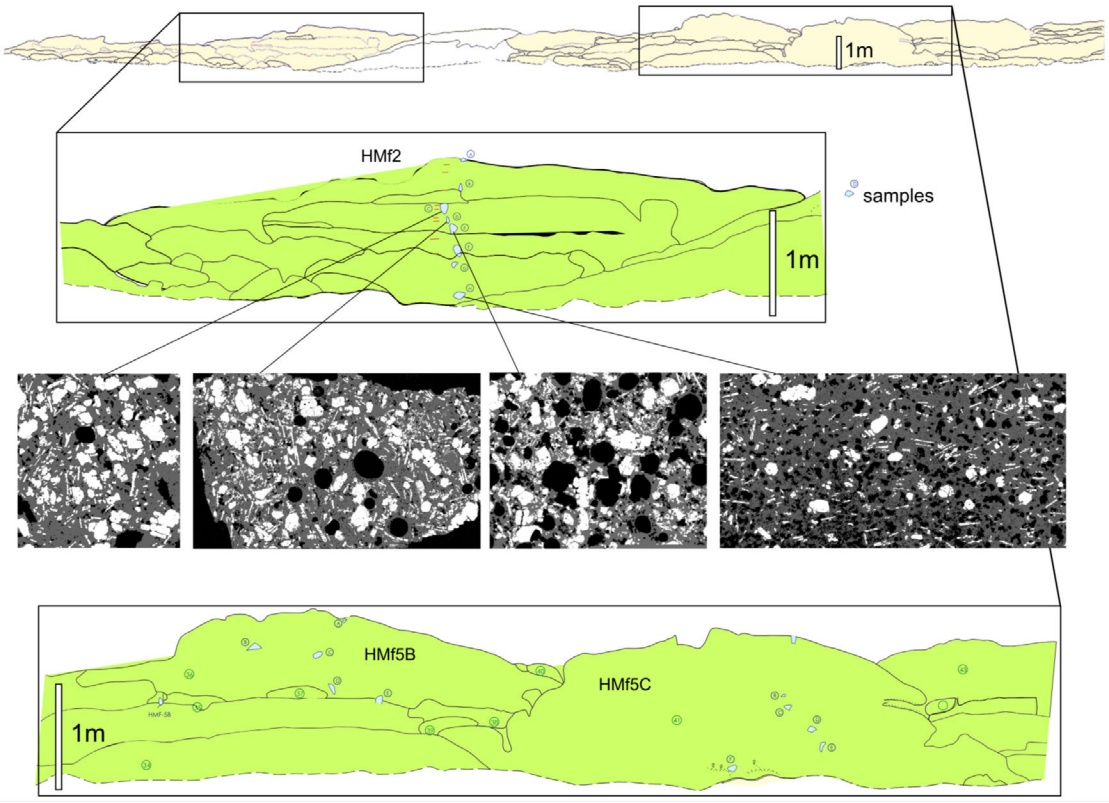

Figure 11: Roadcut map of coast road outcrop C1 (see Figure 1 for location) – overview (top) and detail of the HMF2 sample traverse (center). Images are processed thin sections showing olivine white, vesicles black and groundmass grey, ~2.5 cm on short side.

large volume of crystal and crystal cluster grain size measurements, which is ideally suited to this kind of analysis. However, the number of crystals within individual thin sections are generally not sufficient to yield meaningful PSDs, so we have combined samples in various ways: by locality (vent, Highway and coast road outcrops) and by position of the sample with respect to the flow lobe architecture, e.g. within cores versus lava crusts.

The PSD diagrams that follow plot the log of the number of particles (dendrites or clusters) per unit area (calculated on a vesicle-free basis) within a given size range, normalised against the bin width, against the particle size expressed as equivalent circle diameter, the diameter of a circle with the same area; noting that these are approximations due to stereological effects as described by Higgins [2000] and Higgins [2006]. It was only possible to determine PSDs on glomerocrystic clusters, rather than on individual crystals which make up the clusters. In other words, the measurements represent the size of the crystal clusters, not of individual grains, such that PSD slope cannot be used to draw inferences about residence times or growth rates.

In the case of the olivine plates, the apparent size of the grain depends on whether they are seen side-on or face-on. Most of the sections are cut normal to lobe tops so that the plates are mostly seen side-on; however, because the plates are usually skeletal (Figure 2), single grains often appear in thin section as multiple segments. An attempt was made to carry out stereological corrections for "true" grain size based on the methods of Higgins [2000] and Higgins [2006] and Jerram and Higgins [2007]. However, owing to the highly skeletal nature of the plates and the extreme shape corrections required, we found that results were giving unrealistic artefacts. Similarly, it proved impossible to find an appropriate shape correction applicable to glomerocrysts. We therefore present the data in the plots that follow without stereological correction; they are therefore strictly intersection size distributions, or apparent PSDs, not true PSDs, as should be borne in mind in the following section. Hence, the interpretation of the results is limited to comparing one set of samples with another, such that uncertainties should average out between the groups of samples. The data should not be used to derive quantitative parameters for crystal growth and nucleation rate as can be done with true PSDs.

7.3.1 *Results - overall PSD variations*

Figure 19 shows PSDs for all measured olivine grains in all samples from the 3400 m vent, outcrops 24W and 33 on the Highway, and the C1 outcrop on the coast road. Glomerocrysts and plates define two completely distinct PSD trends, confirming the petrographic observation that these two olivine habits represent distinctly different episodes of nucleation and growth.

The plates have a very high nucleation density and in three of the four datasets have negative slopes, consistent with their

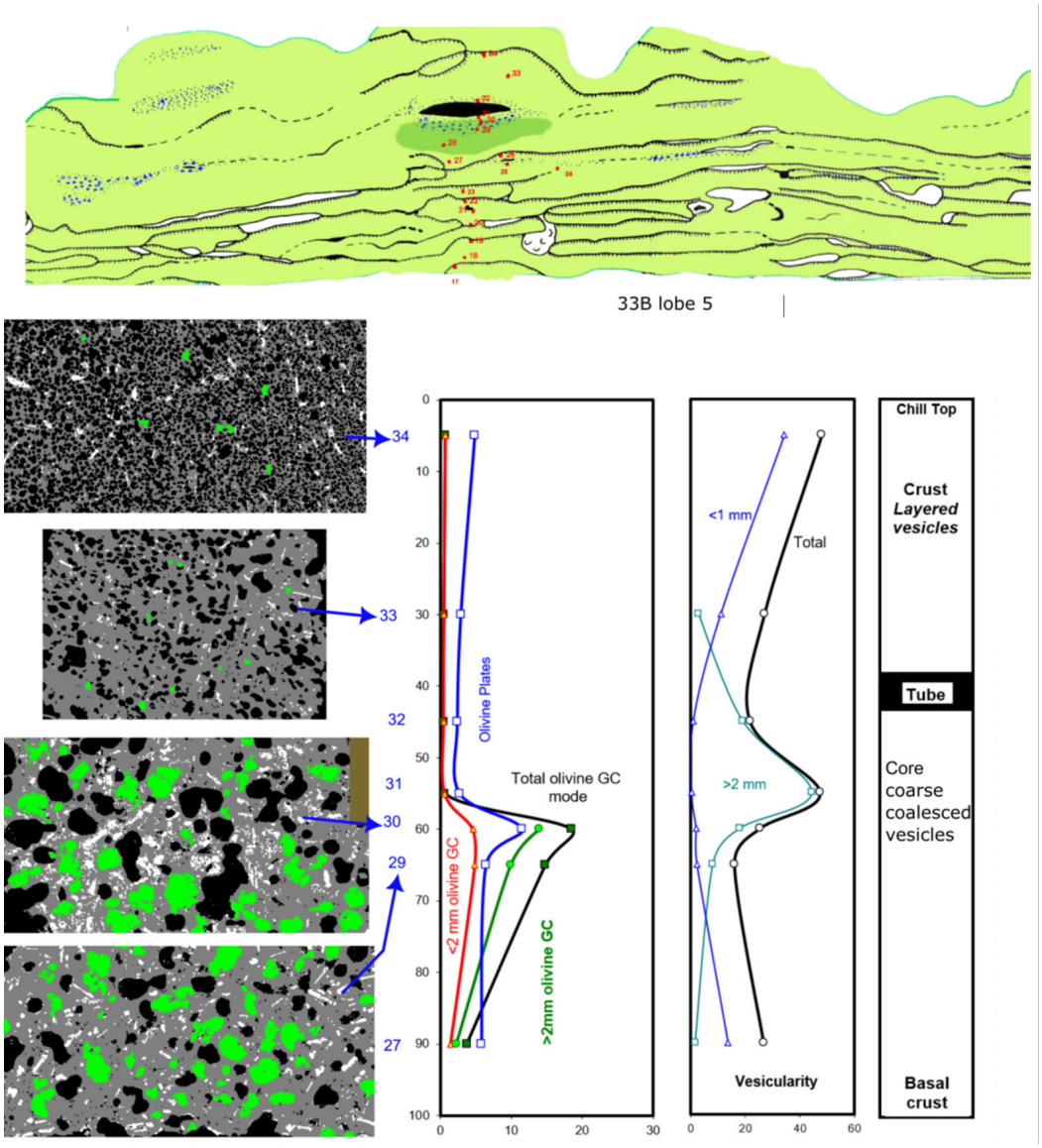

Figure 12: Detailed profile through lobe 33B-5 from the Highway roadcut outcrop 33 (Figure 11). Outcrop sketch shows detailed spatial distribution of samples. Profile shows distribution of olivine plates and glomerocrystic clusters in two different size ranges, <2 mm and >2 mm equivalent circle diameter (ECD). Vesicle distributions are also shown for different size ranges. Thin section images show segmented images of entire thin sections with glomerocrystic olivine in green, plate olivine in white, vesicles black and groundmass in grey. Width of field of view of images ~4 cm.

interpretation as single populations of growing crystals [Cashman and Marsh 1988]. In the case of the glomerocrysts, the clusters define humped distributions that are strongly suggestive of mechanical sorting of crystals, with consideration of the evidence for gravity sorting from the vertical profiles presented above. The composite nature of the glomerocrysts means that the nucleation and growth rate parameters are not meaningful, but as we will see the changes in PSD pattern through the lobes are significant.

7.3.2 *Variation (or otherwise) in PSD of plates*

If the plates have grown significantly during emplacement of the lobes, PSDs of plates should be different in slowly cooled samples from lobe interiors relative to "quenched" samples from lobe margins—they should have the same intercept, but a lower slope. From the data presented in Figure 20A, it appears that this is not the case. PSDs are shown for samples from outcrop 24, subdivided according to the vesicularity; finely vesicular samples from top and bottom crusts, compared with coarse, coalesced vesicle samples from the lobe interior.

Based on these datasets the populations of plates within the different portions of the lobes are very similar. Figure 20B shows that plates from three outcrops—24W and 33B on the Highway, and C1 on the coast road—have similar slopes and nucleation densities (y-intercepts). Coupled with other data presented in this section, the overriding conclusion is that, with the exception of the vent samples, the plate populations are uniform regardless of position in the flow field or within individual lobes. Much of what variability there is probably

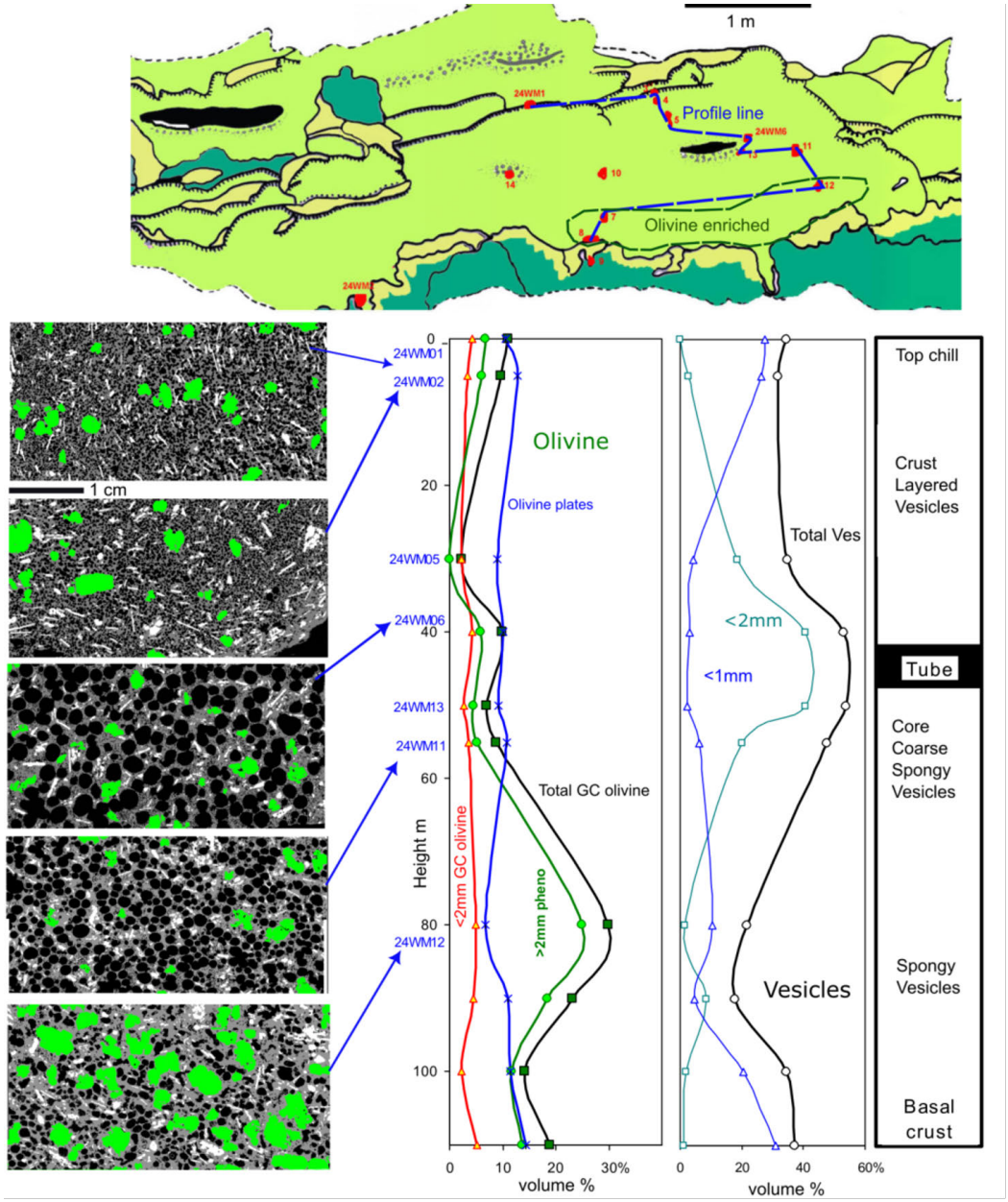

Figure 13: Detailed profile through lobe 24WM-4 from the Highway roadcut outcrops (to the south of outcrop area shown in Figure 9). Profile shows distribution of olivine plates and glomerocrystic clusters in two different size ranges, <2 mm and >2 mm ECD. Vesicle distributions are also shown for different size ranges.

reflects sectioning effects between strongly aligned and randomly oriented plates.

Data for complete olivine populations from ʻaʻā lobes and pāhoehoe lobes from the same roadcut segment are compared in Figure 20C. ʻAʻā lobes are generally deficient in the coarser olivine glomerocryst population, but are identical in the plate population compared with pāhoehoe lobes.

7.3.3 *PSD variations among glomerocrysts in layered lobes*

Figure 20D shows PSD plots for combined olivine data in samples from different parts of layered pāhoehoe lobes in outcrop 24W, representing ~25,000 individual grain measurements. As noted already (Figure 19), PSDs for glomerocrysts show much flatter slopes than those for plates. Given that there is clear evidence in the vertical olivine distribution profiles for mechanical sorting of larger clusters, the slopes of the PSD plots are not meaningful in terms of crystal growth rate. Instead, they reflect the processes which lead to mechanical segregation of large clusters from smaller ones by fluid dynamic processes and crystal settling.

There appears to be no significant difference in the bulk PSDs between samples from upper crusts and from the lava cores. It might be expected that the lobe cores would be systematically enriched in larger olivine clusters relative to the crusts due to crystal settling during flow. As the crust accretes from the top down, it should be sampling lava from which the coarser olivine clusters have preferentially settled into the core lava. This is not evident in the data: the variation in abun-

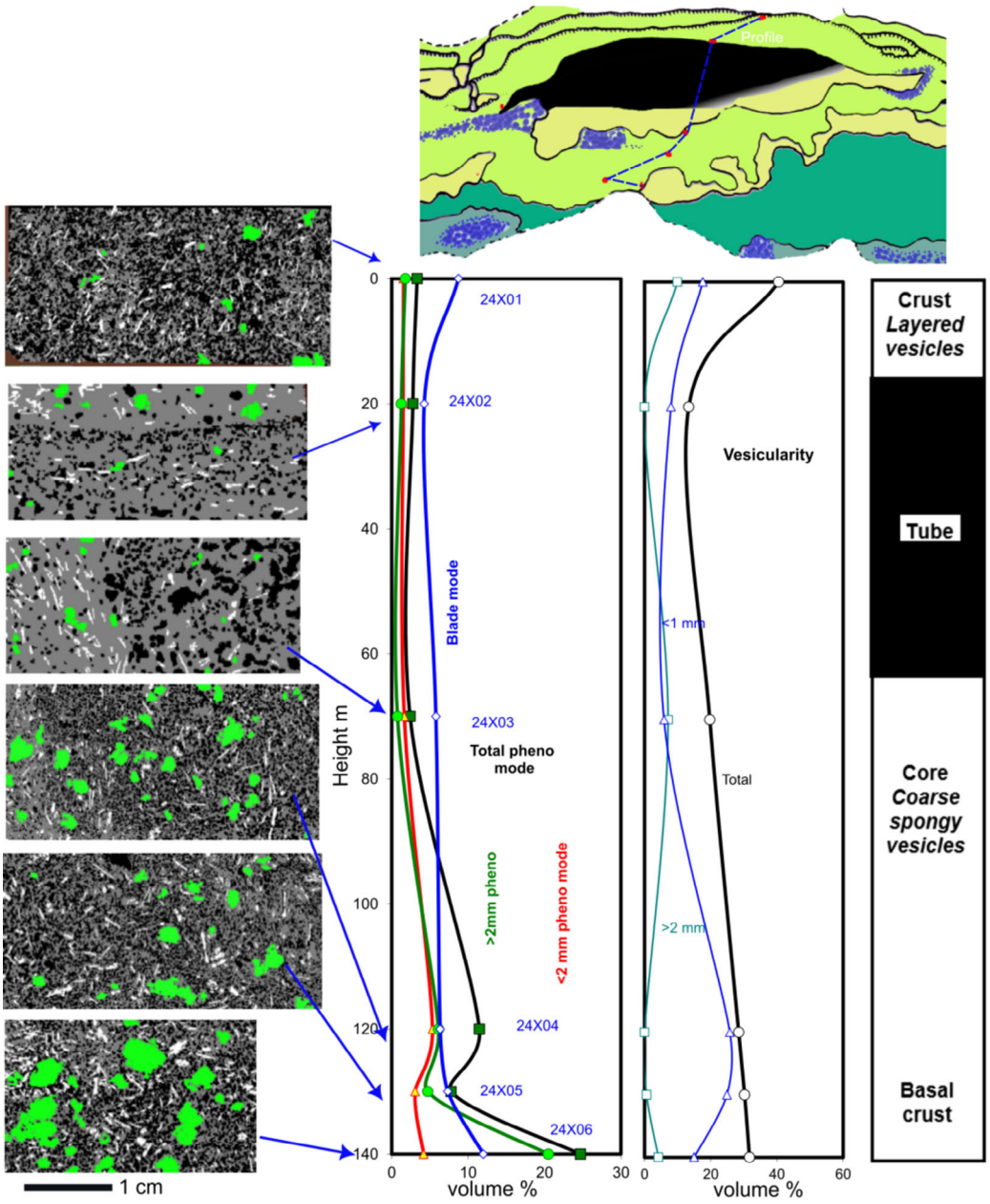

Figure 14: Detailed profile through lobe 24X-4 from Highway roadcut outcrop, as per previous figure. See Figure 9 for outcrop map and detailed location. Profile shows distribution of olivine plates and glomerocrystic clusters in two different size ranges, <2 mm and >2 mm ECD. Vesicle distributions are also shown for different size ranges.

dance of the coarser clusters seems to be happening entirely within the cores, rather than between the cores and crusts.

Figure 20D also shows PSDs for samples from layered pāhoehoe cores only, subdivided according to their glomerocryst content. Olivine-depleted samples are clearly more strongly depleted as the grain size increases, and vice versa for olivine-enriched samples. There is no difference in crystal abundance for glomerocrysts smaller than ~1.5 mm diameter. The implication is that glomerocryst distribution is influenced by grain-size dependent processes, of which the obvious one is crystal settling. The source of most of the variance in glomerocryst distribution is gravitational settling within fluid lobe cores. In the next section we consider the implications of these patterns through a simple computational model.

7.4 Constraints on viscosities and timescales from modelling of Stokes' Law settling

The vertical distribution of olivine grains within single cooling units potentially gives information on the time scale over which crystal settling operated, as well as on effective lava viscosity [Rowland and Walker 1988]. We approach this by modelling the simple bounding case of settling from a static magma column.

A simple finite element model was constructed which takes as its starting point the observed crystal size distribution

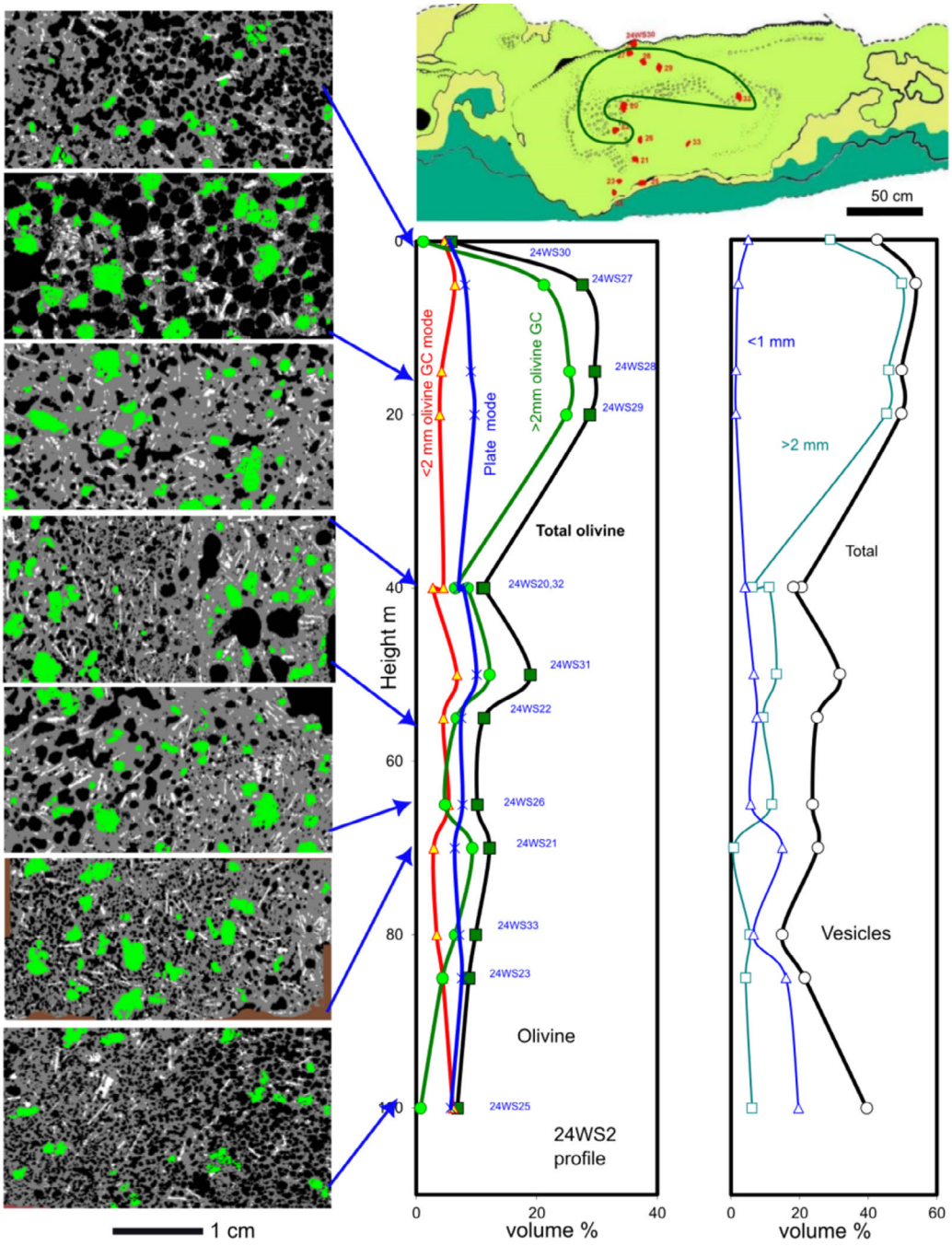

Figure 15: Detailed profile through lobe 24WS-2 from Highway roadcut outcrop (see Figure 9 for detailed location). Profile shows distribution of olivine plates and glomerocrystic clusters in two different size ranges, <2 mm and >2 mm ECD. Vesicle distributions are also shown for different size ranges.

shown in Figure 19 for all combined samples from outcrop 24W and assuming that this population of crystals (or crystal clusters)—many little ones, fewer big ones—is initially distributed evenly and randomly through a static lava column, taken as being 1 m thick. (In this simulation, we apply a systematic correction of +15 % to obtain "true" grain size from apparent PSDs, this being an approximation based on comparing corrected and uncorrected data on a subset of samples using the Higgins method, and assume spherical particles.) With time, these crystals settle at various rates depending on their size (Figure 21). Simultaneously the lobe is cooling, and the front of the viscoelastic crust grows down from the top of the flow and up from the bottom. The advance of the upper crust proceeds as the square root of time and is parameterised as described by Rowland and Walker [1988]. Crystal settling continues until that part of the flow becomes incorporated into the viscoelastic crust, when the crystal profile at that point becomes frozen in. Making some reasonable assumptions about lava viscosity and the propagation rate of the viscoelastic crust (upward from the base and downward from

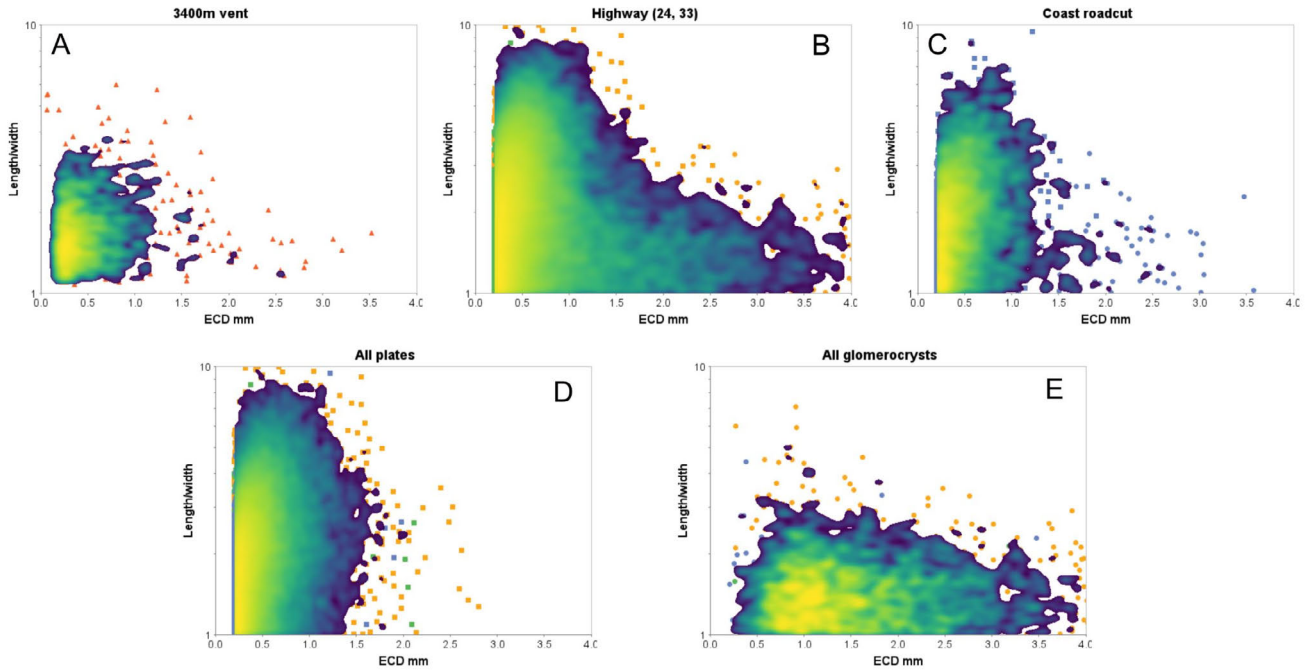

Figure 16: Size–aspect ratio (iogas data density plots)–of grains >0.2 mm ECD only. 47,000 olivine measurements total. [A]–[C] All grains (glomerocrystic clusters and plates) by locality; [D] plates only; [E] glomerocrystic clusters only.

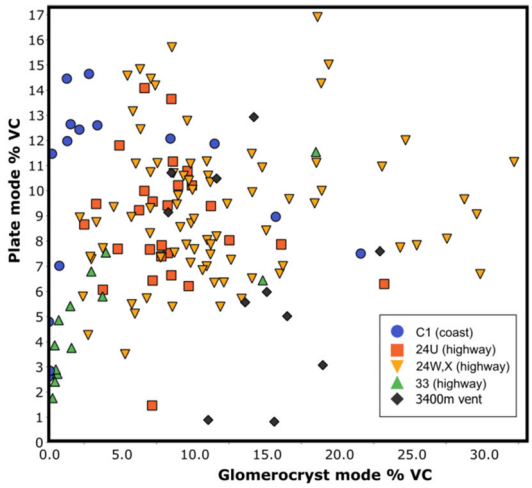

Figure 17: Plot of olivine plate versus glomerocryst mode, vesicle corrected (VC), in individual samples from outcrops 24U (mainly ʻaʻā), 24W and X (Highway traverse – see Figure 1), the 3400 m vent and from the coast road (C1).

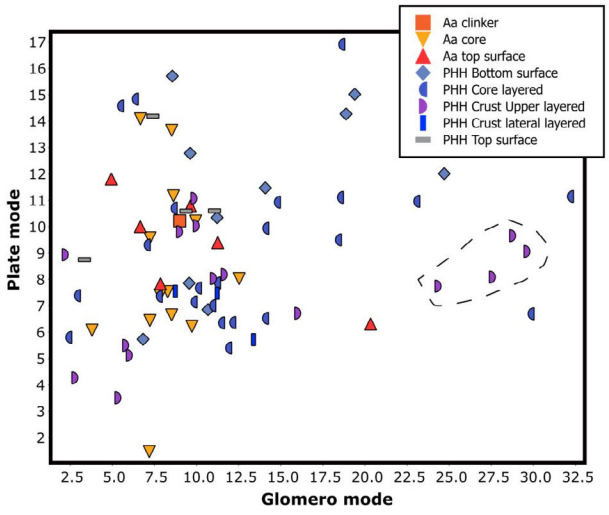

Figure 18: Vesicle corrected modes of glomerocrysts and plates as a function of lobe type and position within outcrop 24. The four upper crust samples taken from a single lobe are outlined in a dashed line.

the top), and starting with a randomly distributed population of 10,000 crystals with the given size distribution profile, it is possible to calculate the final distribution of crystals of various size within the flow at the point of complete solidification (Figure 22). The assumption of spherical particles introduces some uncertainty for the case of the non-spherical clusters, but the effect is likely to be small: the reduction in settling velocity ids of order 10 % for non-spherical particles with aspect ratios of up to 4 [Kerr and Lister 1991].

It should be emphasised that the model shown here represents a simple end-member scenario that ignores the potential effects of inflation, and also ignores possible entrainment within upward-directed eddies or convection currents. An opposite end member would be a situation where the flow lobe is steadily inflating with constant supply of new phenocryst-bearing magma and a steady state crust thickness, such that the crystal-depleted upper part of the lobe is constantly replenished with new magma with the original phenocryst population. The final distribution of crystals would then depend on

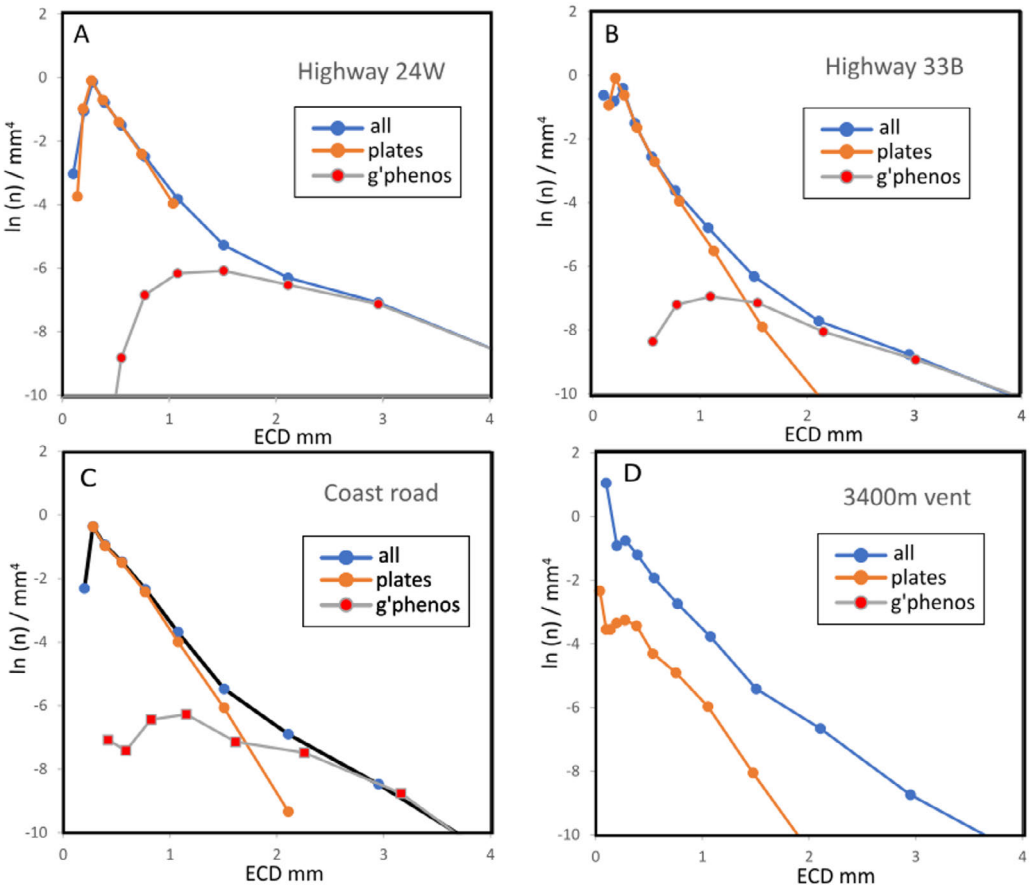

Figure 19: Particle Size Distribution (PSD) plots for different outcrop areas. [A] Highway outcrop 24W, [B] Highway outcrop 33, [C] Honaunau roadcut, coast road, [D] 3400 m vent. "g'phenos" = glomerocrysts (size is for cluster, not individual grains). Size variable on x-axis is Equivalent Circle Diameter (Heywood diameter) of particle intersections viewed in 2D, i.e. not corrected for stereological effects.

the rate of inflation, the rate of flow and the final thickness of the lobe when inflation ceases. Certain combinations could lead to a situation such as that shown in Figure 15D where there is no downward concentration of olivine at all.

Nevertheless, the simple static model provides some useful constraints on viscosities and timescales. The first conclusion is that in order to account for the degree of differential settling of the coarse olivine clusters effective viscosities must have been of the order of 1000 Pa s, towards the upper end for field measurements in active Mauna Loa flows, which range from 140 Pa s at eruption to 1400 Pa s downstream [Moore 1987]. The higher values are more than an order of magnitude higher than calculated viscosities for Moinui glass compositions at their liquidus temperature of around 20–50 Pa s, based on the viscosity calculator of Giordano et al. [2008] (Table 1), the difference being probably attributable to the high proportion of vesicles.

The more important conclusion for present purposes is that the timescale for settling of coarse crystals to produce typical Moinui profiles, such as those seen in Figure 12 and Figure 13, is comparable to the timescale for cooling of an entire 1 m thick lobe to the holding isotherm, which is around 2–3 days. This is at the low end of diffusion chronometry estimates for the timescale of formation of the olivine plates [Couperthwaite et al. 2020]. This further implies that the timescale for flow of lava through individual pathway networks from the vent to the ocean was similar to the timescale for development of the settling profiles, i.e. a few days, broadly consistent with measurements of active tube-fed flows on Kīlauea [Mattox et al. 1993; Kauahikaua et al. 1998]. If flow had taken significantly longer, then, noting that the downward settling velocity and the horizontal transport velocity are entirely independent of one another, crystal settling upstream in the distributary tubes would have depleted the flow in coarse olivine clusters and there should be a significant drop-off along the length of the flow. There is in fact a small drop-off between the Highway and coast road samples, suggesting that some accelerated settling and depletion of olivine may have occurred at break of slope between the oceanward slope of the volcano and the narrow coastal plain where the coast road samples are located.

8 Discussion

8.1 Redistribution of crystal populations in propagating flow lobes

The data presented here on olivine distributions imply that redistribution of crystal populations within individual flow lobes

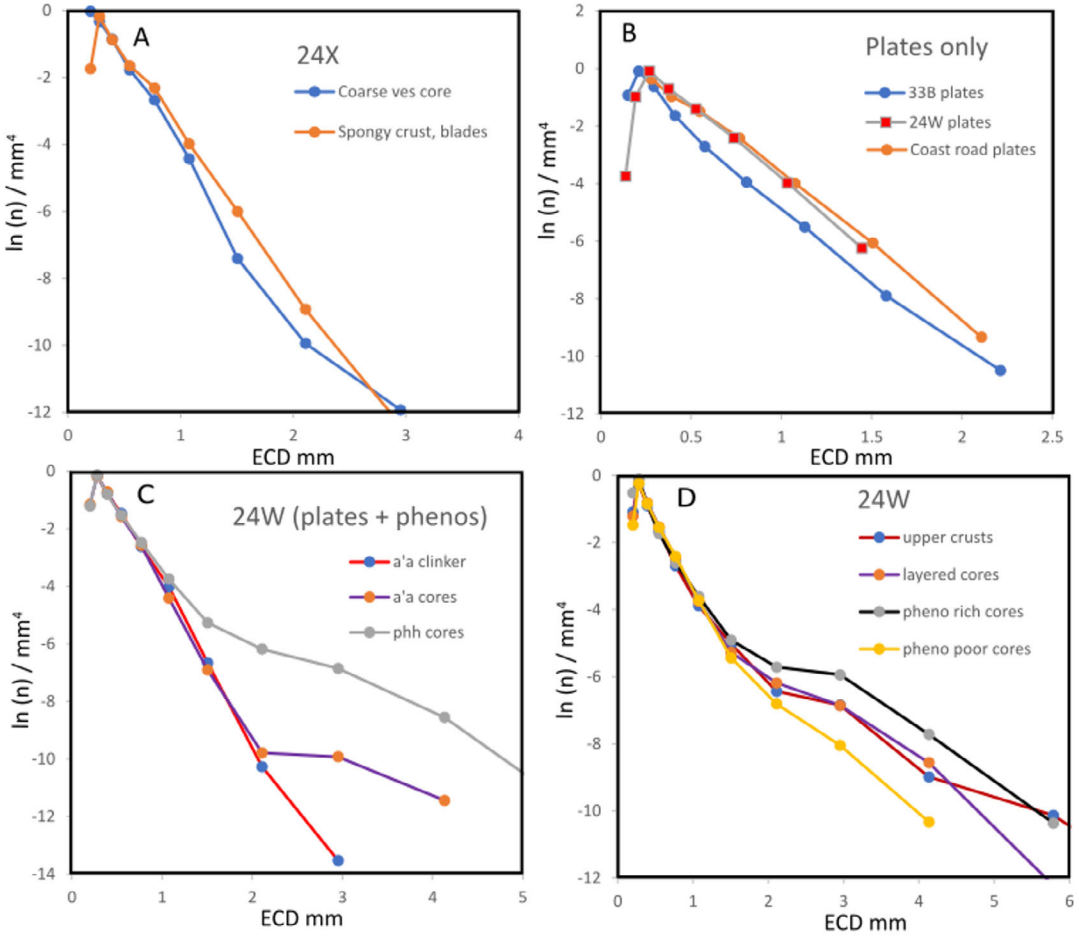

Figure 20: [A] Crystal size distribution plots (strictly, intersection size, as these are not corrected for stereological effects) for olivine plates from outcrop 24X, subdivided by style of vesicularity of the sample; coarse vesicular core versus spongy vesicular crust. [B] Same plot for olivine plates only, for all samples subdivided by outcrop (33B, C1 and 24W). [C] ʻAʻā versus pāhoehoe lobes. [D] Plot for all olivines, clusterd samples from outcrop 24W subdivided by position within lobe.

is restricted to cooling units greater than ~1 m in thickness on timescales of days. However, as is evident from Figure 19, samples containing more than ~10 % glomerocrystic olivine are as likely to be found in lobe crusts as in cores and are not restricted to accumulation zones at the bottom of thicker cooling units. We ascribe this relationship to an interplay of inflation and break-out of new lobes during propagation of the flow front and flow-through in established distributary pathways (Figure 23), giving rise to the diversity in olivine and vesicle distribution profiles shown in Figure 12 to Figure 15. Progressive settling of larger grains on timescales of days caused olivine to accumulate downward, but frontal breakout of new lobes from the bottom of existing pathways could lead to the development of thin flanking lobes with high olivine contents (Figure 23E) and high olivine contents in the initial toe-like protrusions, as in lobe 24X-4 shown in Figure 13. Surface breakouts tended to sample material from which the coarser olivine had already settled.

The olivine distribution profile in Outcrop 24WS lobe 2 (Figure 15) is indicative of the complex interplay of these processes. We interpret this profile as the result of the interaction of inflation, changing rate of supply of olivine-enriched lava and growth of the upper crust. Glomerocryst-enriched lava was emplaced early, becoming incorporated into the crust, which was then inflated and lifted by less olivine-rich lava subsequently flowing underneath it.

The general pattern of glomerocryst distribution measured in the various profiles can also be considered in relation to the hypothesis of phenocryst redistribution by flow differentiation, in which suspended particles migrate towards the centre of flow channels due to a type of particle-particle interaction called the Bagnold Effect [Barriere 1976]. We see no evidence of systematic concentration of olivine in the middle of the thinner low lobes, as would be expected if this effect were operating. This is not surprising: the treatment by Barriere [1976] shows that the lengthscale of inward particle translations due to this effect are of the order of cm per hour [Barnes et al. 2018], so would be negligible on the timescales for flow emplacements indicated by the Stokes settling models. Gravity settling appears to the dominant mode of olivine concentration.

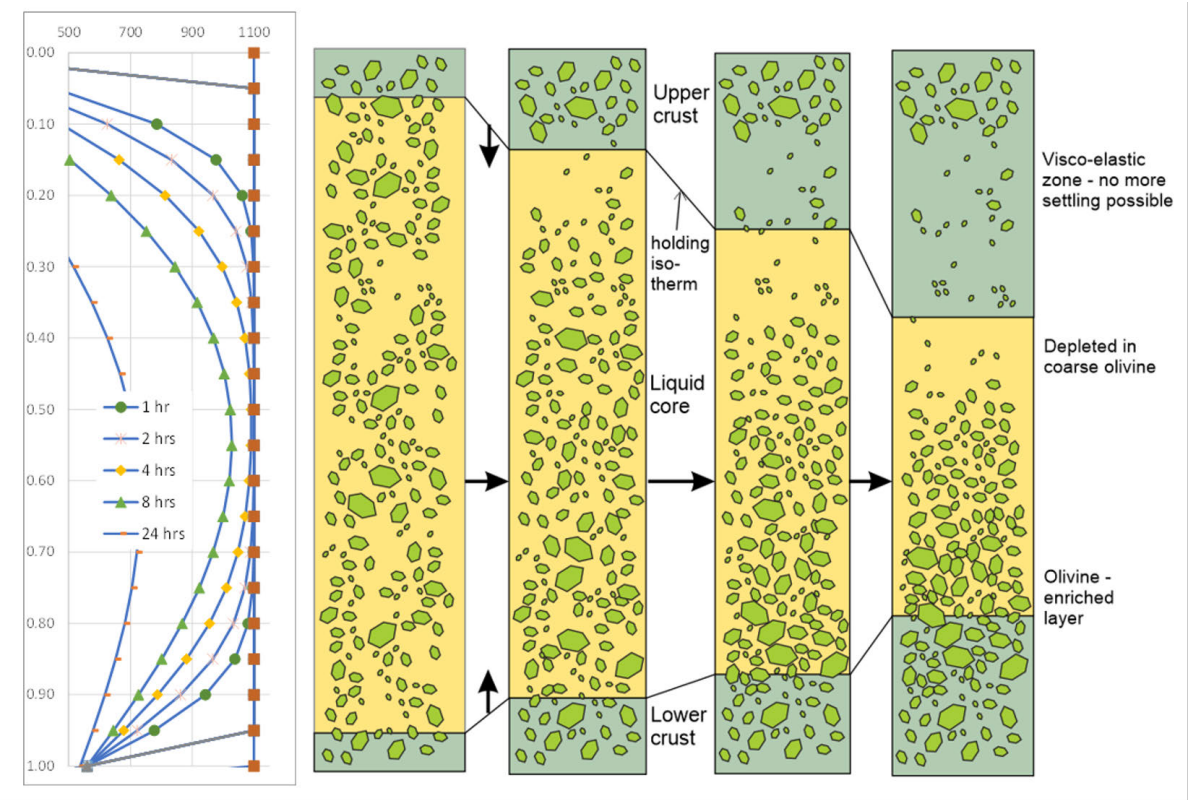

Figure 21: Cartoon illustrating principal of the Stokes Law settling model.

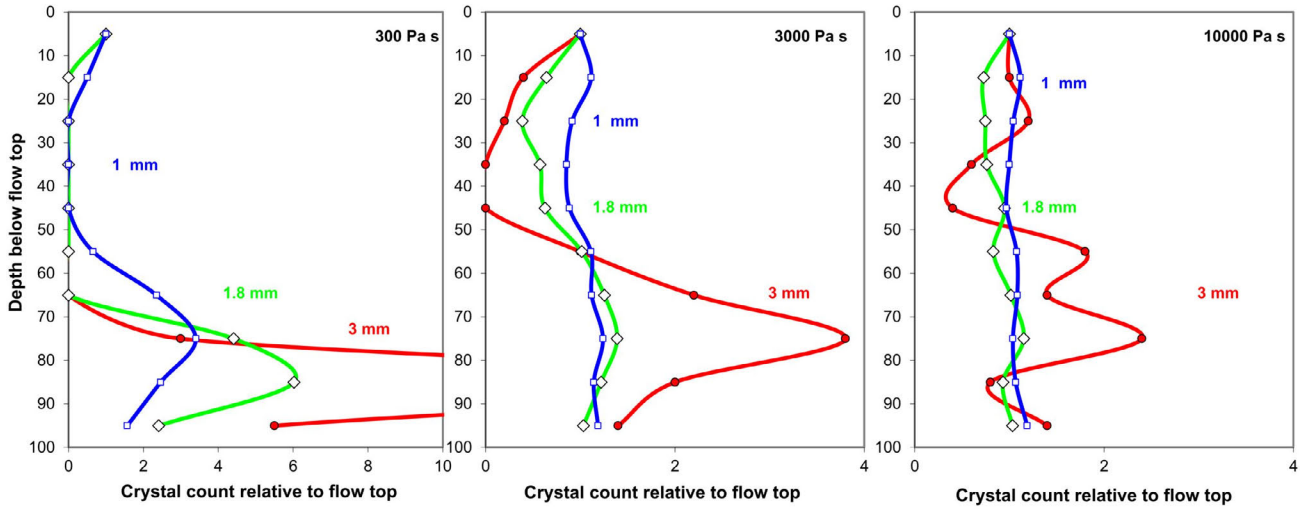

Figure 22: Output of finite element settling model for different values of viscosity, showing distribution with height in the column (y-axis). Coloured curves show distribution of olivine grains in different size ranges. Concentrations are shown relative to the initial concentration frozen into the top of the crust.

8.2 Origin of platy olivine

Couperthwaite et al. [2020] concluded on evidence from diffusion chronometry that the platy olivine population (Fo_{83-82}) nucleated a significant time after entrainment of the glomerocrystic olivine cores and commencement of their diffusive re-equilibration, either during final stages of magma ascent or during the eruption, and equilibrated on a time scale of 2–40 days. Degassing of the melt during ascent and at the surface would have played a major role in rapidly undercooling the melt [Guilbaud et al. 2007], giving rise to a burst of heterogeneous nucleation of skeletal grains, possibly aided by heterogeneous nucleation on gas bubbles. These platy grains were then transported and dispersed through the flow field without undergoing significant further growth. It appears there was relatively little nucleation of dendrites on extant olivine grains, although some of the larger grains do have higher Mg

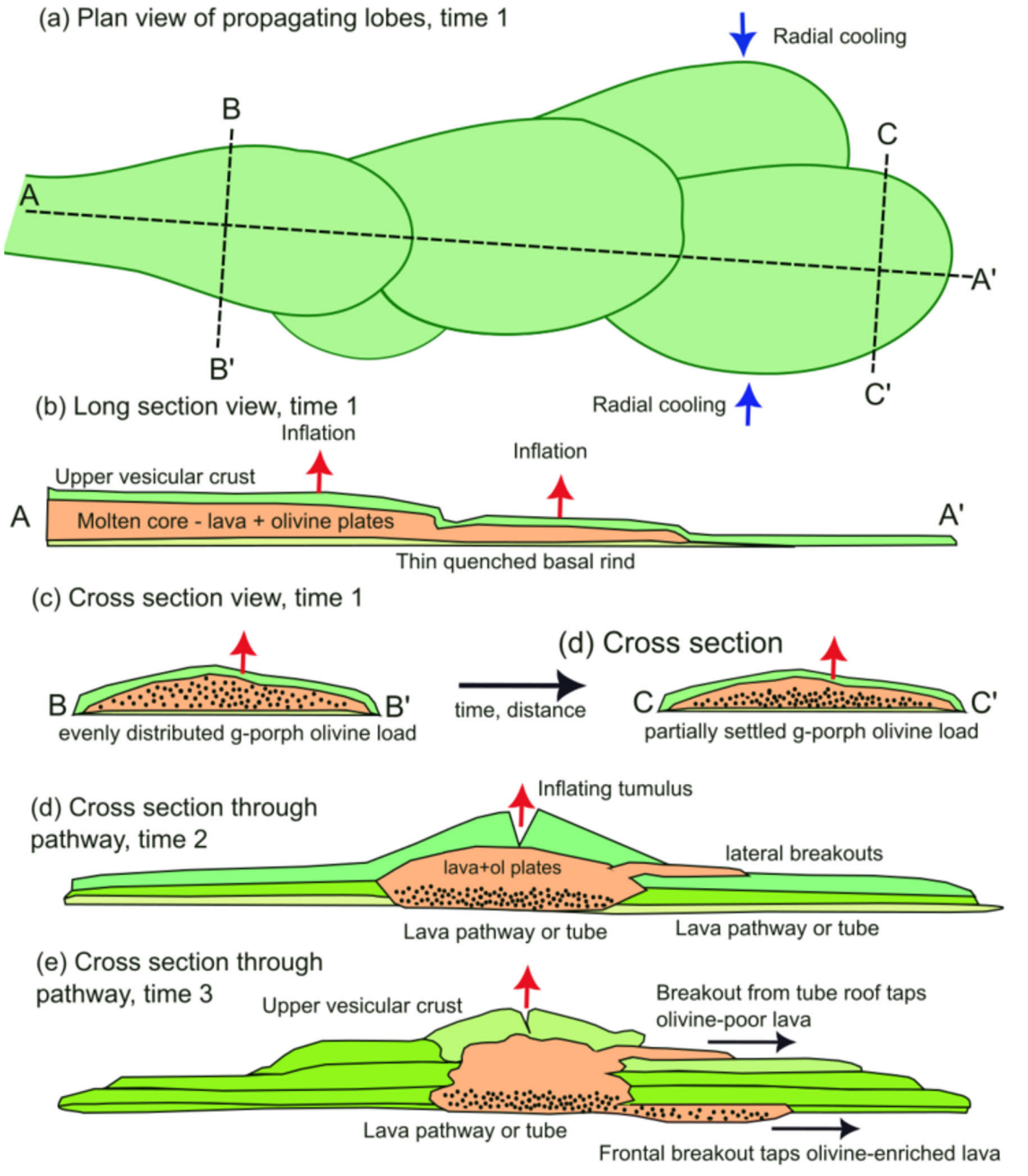

Figure 23: Cartoon for development of flow lobes and redistribution of olivine within the Moinui Flow field, envisaged as a series of interconnected inflating pathways and flanking sheet lobes. Modified from [Hill 2001].

cores (e.g. Figure 2E) implying this origin. Some dendrites are in contact with clusters (Figure 7) but this is could well be due to accidental impingement rather than nucleation.

8.3 Origin of glomerocrystic olivine

Diffusion chronometry data [Couperthwaite et al. 2020] indicate residence times of the glomerocrystic clusters in the transporting magma of the order of a few months to a few years, much greater than the timescale for crystal settling implied by the observed profiles of vertical grain size and modal proportion. This implies that the diffusive ~100s of days timescales relate to storage in the pre-eruption reservoir post-entrainment rather than to post-eruption flow. Similarity of size and crystal numbers in the glomerocrystic clusters between the vent and the distal coast-road outcrops, coupled with the pattern of zoning of olivine in the clusters, further argues against aggregation of olivine crystals by random collision (synneusis)

during post-eruption flow. However, this says nothing about the mechanism of pre-eruption cluster formation.

As noted above, there are several hypotheses for the origins of crystal clusters in igneous rocks: by accidental collisions and adhesion (synneusis) of crystals suspended in flowing magma [Schwindinger and Anderson 1989; Wieser et al. 2019], by processes of heterogeneous self-nucleation [Campbell 1978; Latypov et al. 2022], or by entrainment and disaggregation of pre-existing subvolcanic cumulates [Dowty 1980; McIntire et al. 2019], or by poorly understood processes such as secondary nucleation, known in the crystal growth literature but as-yet unrecognised in igneous petrology [Anwar et al. 2015].

In a pioneering study of 3D textures in igneous rocks, Philpotts and Dickson [2000] imaged clusters of plagioclase in dolerites, and used the relationship between zoning and contact points to argue that the grains must have had a period of growth while freely suspended before impinging on one another in the magma; the contact points between the grains are between the relatively low-An outer rims. On this basis Philpotts and Dickson [2000] argued for a synneusis origin. However, it is important to note that these observations were made in 2D section. Inspecting the relationship between Mg-Fe zoning in our olivine clusters in the 3D image, we observed that around 85 % of touching olivine-olivine grain pairs have mutual contacts between Mg-rich cores, with the remainder having contacts only between Fe-rich rims. This is not immediately apparent looking only at 2D sections, in which a much higher proportion of grains appear to impinge only at the rims. These relatively Mg-rich cores are out of equilibrium with the transporting magma but were formed months to years before eruption [Couperthwaite et al. 2020]; it follows that the clusters must also have formed at this time. Hence, if they did form by the random-collision synneusis mechanism, they must have done so while suspended in a convecting or flowing magma, richer in MgO than the Moinui lava, within the sub-volcanic plumbing system, then have subsequently been entrained by the Moinui lava.

Table 1: Typical electron microprobe analyses of glass in margin of flow lobe from the C1 (coast) outcrop, normalised to 100 % for different water contents. Viscosities determined using the silicate melt viscosity calculator of [Giordano et al. 2008].

	HMF1-1	HMF1-2	HMF1-3
SiO_2	52.60	52.34	51.81
TiO_2	2.30	2.30	2.30
Al_2O_3	14.03	13.96	13.82
FeO(T)	9.77	9.72	9.62
MnO	0.15	0.15	0.15
MgO	6.76	6.73	6.66
CaO	10.92	10.87	10.76
Na_2O	2.35	2.34	2.32
K_2O	0.41	0.41	0.40
P_2O_5	0.20	0.20	0.20
H_2O	**0.50**	**1.00**	**2.00**
η pa s 1000 °C	2147.6	906.7	366.1
η pa s 1100 °C	261.3	133.1	64.2
η pa s 1200 °C	49.3	28.7	15.7

An alternative is that the olivine clusters were xenocrysts—"tramp crystals" in the terminology of Marsh [2015]—generated by disruption and entrainment of cumulates generated at some indeterminate point in the sub-volcanic plumbing system. This conclusion is consistent with that of McIntire et al. [2019], based on computational fluid dynamic modelling, that crystal cargo suites exhibiting a dominance of crystal clusters are more likely to be sampling magmatic materials formed in a crystal mush than to have formed by random collision.

A further test of alternative hypotheses is the gain-scale microstructure within the clusters. The predominant feature is presence of multiple grains in similar but slightly displaced orientations (e.g. Figure 4C, D, H), with smooth curved grain boundaries and in (relatively infrequent cases) 120° triple point boundaries (Figure 4A, F) indicating approach towards textural equilibrium. This latter feature would favour formation in a cumulate pile in a subvolcanic intrusion, but the more common observation of multiple misoriented subgrains (Figure 4F) is not at all typical of magma chamber cumulates. The presence of grains containing misoriented lamellae (Figure 4E, G) is suggestive of within-grain deformation, which would indicate formation in a compacting crystal mush. The common presence of small grains partially or completely enclosed in large ones implies continuing grain growth following initial contact. The presence of relatively rare polymineralic inclusions (Figure 4E) is suggestive of sampling a mush. Hence, the evidence is somewhat conflicting and it is likely that there is no single origin.

Wieser et al. [2019] report olivine clusters from Kīlauea lavas with very similar attributes to ours, particularly showing multiple slightly misoriented grains in face contact. On the basis of crystal orientation evidence, they rejected origins by overgrowth of dendrites and argued for synneusis, i.e. aggregation by random collision of suspended grains. As we have argued above, if this is the correct mechanism then it must have taken place in a different magma than the one in which the clusters are now entrained, and on a timescale of years before their eruption. Further, it is by no means clear why random aggregation of suspended grains would lead to the strongly preferred common orientations of grains within clusters; Wieser et al. [2019] suggest this is controlled by hydrodynamic sorting into preferred grain orientations, a feature for which we see no evidence in natural cumulates or in the olivine-rich Moinui Flow lobes. Alternative explanations involving heterogeneous nucleation, possibly involving the as-yet poorly understood process of secondary nucleation [Anwar et al. 2015] require further investigation. The ubiquitous presence of small chromite grains within the clusters may also be significant. Heterogeneous nucleation of olivine on chromite, or vice versa, would answer the criticism by Holness et al. [2022] that self-nucleation is impossible on thermodynamic grounds. The apparently conflicting evidence from the microstructures could be reconciled by forming the clusters initially by heterogeneous nucleation and growth pro-

cesses while suspended in a (now unsampled) magma, followed by localised settling into a crystal mush and subsequent re-entrainment by the Moinui magma months or years prior to eruption. The problem remains unsolved in our view. Detailed investigation of crystal orientations is underway on the Moinui clusters using 3D diffraction tomography and will be presented in a companion paper.

9 Conclusions

Our major conclusions are presented here in relation to the questions posed in the Section 1.

9.1 Internal architecture and emplacement mechanisms

The Moinui lava was erupted as a compound flow field, fed by distributary pathways of the order of 50–150 cm thick and 2–10 m wide, associated with flanking breakouts a few 10s of cm thick. The position of the thick, relatively slow-cooled pathways is marked by low vesicle content, coalescence and growth of vesicles and downward settling of suspended olivine glomerocrysts. The internal flow architecture is dependent on the slope of the substrate. The distal portion of the flow field, emplaced on the horizontal coastal plain, shows broader, thicker lobes, a smaller proportion of multiple thin breakouts, and more extensive development of inflationary tumuli. Furthermore, the overall proportion of glomerocrystic olivine appears somewhat lower. This may be due to preferential settling or winnowing of the olivine clusters at the break of slope. A small proportion of the thicker lobes developed on the oceanward slope (i.e. in the Highway roadcuts) show flat-bottomed drainage cavities, transitional into true tubes. These form when there is a slight pressure drop within the transport system such that the lava moving through the pathway cannot maintain enough overpressure to keep the chamber full to the brim. In contrast, the mostly tube-free tumuli on the coast road form when the inflow is greater than the outflow, causing continuous inflation of the tube roof [Hon et al. 1994; Self et al. 1996; Thordarson and Self 1998].

9.2 Origin of the glomerocrysts

The olivine glomerocryst clusters show development of Fe-rich outer rims, mainly developed around the margins of the clusters rather than around the individual component grains (Figure 2, Figure 6), indicating that the clusters were already formed prior to the crystallisation of the rims. These rims match the compositions of the plates, indicating that they also developed during or immediately post-eruption.

Glomerocryst assemblages are remarkably similarly in their cluster size distributions throughout the entire flow field. This further indicates that they were entrained as clusters within the lava at the time of eruption, retained their integrity along a 32 km flow path and survived the processes of flow, inflation and breakout formation. If they were formed by a process of random collision and synneusis [Vance 1969; Schwindinger and Anderson 1989; Wieser et al. 2019] then this process must have preceded eruption and must have taken place in a different carrier magma. Textural evidence from the glomerocryst clusters is ambiguous, and the question of their ultimate origin remains open.

9.3 Growth, settling, and physical redistribution of the olivine cargo

The Moinui lava was erupted with approximately 5–10 % olivine glomerocrysts and about the same proportion of dendritic plates. The similarity of platy olivine populations between lobe crusts and cores implies that only minor additional growth of plates occurred after an initial burst of supercooled growth, probably caused by a degassing episode during eruption; the entire platy-olivine population behaved essentially as a passive transported load throughout development of the flow field. Olivine plates are uniformly distributed throughout pāhoehoe and ʻaʻā lobes and show no systematic concentration. There is only a very limited tendency for plates to settle in lobes where the glomerocryst population has clearly settled. There is no evidence of systematic concentration of olivine in the centres of thin lobes, as would be suggestive of Bagnold Effect flow differentiation [Barriere 1976]. Rather, the dominant control on olivine glomerocryst distribution is simple gravitational settling. This is the only explanation for the preferential downward concentration of larger but not smaller grain clusters. Much (but not all) of this settling must have postdated inflation and crust accretion, to account for the fact that pāhoehoe crusts as a whole are not depleted in coarse olivine clusters relative to the cores of layered lobes. Olivine clusters are evidently very stable during flow, even on steep slopes. Furthermore, apart from growth of a part of the plate population, and possibly of the outermost Fe-rich rims on the glomerocrysts, there was limited olivine crystal growth during flow.

Crystal sorting of glomerocrysts in pāhoehoe lobes is a function of grain size; significant degrees of crystal settling for the most part only happen in the +2 mm grain-cluster size fraction and are most evident in the thicker lobes (greater than 1 m). However, lobe cores are not systematically enriched in glomerocrysts relative to crusts.

The major tumuli or pathways are not systematically enriched in glomerocryst olivine relative to flanking spongy lobes, although they show greater internal differentiation due to settling. They may contain olivine accumulations, but these are balanced by overlying zones of olivine depletion. The same lack of contrast applies to the plate population. This implies that both olivine populations were distributed evenly through the flow field by the combined processes of inflation, tube and tumulus formation, and lateral or frontal breakouts. The process of accumulation into olivine enriched zones probably took place either during flow within the established pathways, or immediately post-stagnation.

9.4 Time-scale and effective lava viscosity estimates

The lack of settling of plates and smaller glomerocrysts suggest that the lavas had effective average viscosities of around 1000 Pa s at the stage where crystals were settling; this is a higher value than expected for the lava composition at its liquidus temperature, the difference being attributable to the crystal and vesicle load. Olivine distribution is consistent with emplacement and cooling to non-Newtonian conditions on time scales of ten of hours to a few days. There is no olivine settling at all in ʻaʻā lobes, despite their having a similar overall

olivine population to the neighbouring pāhoehoe lobes, consistent with the ʻaʻā lava having a significantly greater viscosity and/or yield strength [Belousov and Belousova 2017].

Author Contributions

Barnes: wrote the manuscript, mapped and sampled outcrops, collected and interpreted image processing data. Thordarson: mapped and sampled outcrops, contributed to writing. Hill: initiated the study, mapping and sampling. Perring: mapping, sampling, image processing. Dowling: mapping and sampling. Godel: MicroCT data collection and 3D image processing.

Acknowledgements

We dedicate this paper to the memory of Dr James Kauahikaua (Jim K) who introduced us to the Moinui exposures and contributed his wealth of expertise and knowledge of Hawaiian volcanism to this project. He also collected the 3400 m vent samples. Jim was the first native Hawaiian director of the Hawaiian Volcano Observatory (HVO) and a vital contributor to knowledge of the volcanology of the Big Island. We also thank HVO for their hospitality and assistance over several field visits. The XRF element maps were collected at the XFM beamline of the Australian Synchrotron in Clayton, Victoria, part of ANSTO. Morgan Williams assisted with `MELTS` modelling, Stefano Caruso with CT data processing and Michael Verrall with 2D image processing. Rais Latypov and Tari Mattox kindly offered suggestions for improvement on an early draft. We thank Marian Holness and an anonymous referee for stimulating discussion and helpful suggestions.

Data Availability

The full dataset used in this publication is available for download as a `Microsoft Access` database from the CSIRO public data access portal at `https://data.csiro.au/collection/csiro:61210`.

Copyright notice

References

Anderson, A. T., G. H. Swihart, G. Artioli, and C. A. Geiger (1984). "Segregation Vesicles, Gas Filter-Pressing, and Igneous Differentiation". *The Journal of Geology* 92(1), pages 55–72. ISSN: 00221376, 15375269.

Anwar, J., S. Khan, and L. Lindfors (2015). "Secondary Crystal Nucleation: Nuclei Breeding Factory Uncovered". *Angewandte Chemie International Edition* 54(49), pages 14681–14684. ISSN: 1521-3773. DOI: 10.1002/anie.201501216.

Aubele, J. C., L. Crumpler, and W. E. Elston (1988). "Vesicle zonation and vertical structure of basalt flows". *Journal of Volcanology and Geothermal Research* 35(4), pages 349–374. ISSN: 0377-0273. DOI: 10.1016/0377-0273(88)90028-5.

Barnard, W. M. (1995). "Mauna Loa Volcano: Historical eruptions, exploration, and observations (1779–1910)". *Geophysical Monograph Series*. American Geophysical Union, pages 1–19. ISBN: 0875900496. DOI: 10.1029/gm092p0001.

Barnes, S. J., M. Le Vaillant, B. Godel, and C. M. Lesher (2018). "Droplets and Bubbles: Solidification of Sulphide-rich Vapour-saturated Orthocumulates in the Norilsk-Talnakh Ni–Cu–PGE Ore-bearing Intrusions". *Journal of Petrology* 60(2), pages 269–300. ISSN: 1460-2415. DOI: 10.1093/petrology/egy114.

Barnes, S. J., A. R. Cruden, N. Arndt, and B. M. Saumur (2016). "The mineral system approach applied to magmatic Ni–Cu–PGE sulphide deposits". *Ore Geology Reviews* 76, pages 296–316. ISSN: 0169-1368. DOI: 10.1016/j.oregeorev.2015.06.012.

Barnes, S. J. and J. C. Robertson (2019). "Time scales and length scales in magma flow pathways and the origin of magmatic Ni–Cu–PGE ore deposits". *Geoscience Frontiers* 10(1), pages 77–87. ISSN: 1674-9871. DOI: 10.1016/j.gsf.2018.02.006.

Barriere, M. (1976). "Flowage differentiation: Limitation of the "Bagnold effect" to the narrow intrusions". *Contributions to Mineralogy and Petrology* 55(2), pages 139–145. ISSN: 1432-0967. DOI: 10.1007/bf00372223.

Belousov, A. and M. Belousova (2017). "Dynamics and viscosity of 'a'a and pahoehoe lava flows of the 2012–2013 eruption of Tolbachik volcano, Kamchatka (Russia)". *Bulletin of Volcanology* 80(1). ISSN: 1432-0819. DOI: 10.1007/s00445-017-1180-2.

Campbell, I. (1978). "Some problems with the cumulus theory". *Lithos* 11(4), pages 311–323. ISSN: 0024-4937. DOI: 10.1016/0024-4937(78)90038-5.

Cashman, K. V. and B. D. Marsh (1988). "Crystal size distribution (CSD) in rocks and the kinetics and dynamics of crystallization II: Makaopuhi lava lake". *Contributions to Mineralogy and Petrology* 99(3), pages 292–305. ISSN: 1432-0967. DOI: 10.1007/bf00375363.

Costa, F. and M. Dungan (2005). "Short time scales of magmatic assimilation from diffusion modeling of multiple elements in olivine". *Geology* 33(10), page 837. ISSN: 0091-7613. DOI: 10.1130/g21675.1.

Couperthwaite, F. K., T. Thordarson, D. J. Morgan, J. Harvey, and M. Wilson (2020). "Diffusion Timescales of Magmatic Processes in the Moinui Lava Eruption at Mauna Loa, Hawai'i, as Inferred from Bimodal Olivine Populations". *Journal of Petrology* 61(7). ISSN: 1460-2415. DOI: 10.1093/petrology/egaa058.

Dowty, E. (1980). "Synneusis Reconsidered". *Contributions to Mineralogy and Petrology* 74(1), pages 75–84. ISSN: 1432-0967. DOI: 10.1007/bf00375491.

Ganne, J., O. Bachmann, and X. Feng (2018). "Deep into magma plumbing systems: Interrogating the crystal cargo of volcanic deposits". *Geology* 46(5), pages 415–418. ISSN: 0091-7613. DOI: 10.1130/g39857.1.

Giordano, D., J. K. Russell, and D. B. Dingwell (2008). "Viscosity of magmatic liquids: A model". *Earth and Planetary Science Letters* 271(1–4), pages 123–134. ISSN: 0012-821X. DOI: 10.1016/j.epsl.2008.03.038.

Godel, B. (2013). "High-Resolution X-Ray Computed Tomography and Its Application to Ore Deposits: From Data Acquisition to Quantitative Three-Dimensional Measurements with Case Studies from Ni-Cu-PGE Deposits". *Economic Geology* 108(8), pages 2005–2019. ISSN: 1554-0774. DOI: 10.2113/econgeo.108.8.2005.

Gole, M. J. and S. J. Barnes (2020). "The association between Ni-Cu-PGE sulfide and Ni-Co lateritic ores and volcanic facies within the komatiites of the 2.7 Ga East Yilgarn Craton Large Igneous Province, Western Australia". *Ore Geology Reviews* 116, page 103231. ISSN: 0169-1368. DOI: 10.1016/j.oregeorev.2019.103231.

Guilbaud, M.-N., S. Blake, T. Thordarson, and S. Self (2007). "Role of Syn-eruptive Cooling and Degassing on Textures of Lavas from the AD 1783-1784 Laki Eruption, South Iceland". *Journal of Petrology* 48(7), pages 1265–1294. ISSN: 1460-2415. DOI: 10.1093/petrology/egm017.

Higgins, M. D. (2000). "Measurement of crystal size distributions". *American Mineralogist* 85(9), pages 1105–1116. ISSN: 0003-004X. DOI: 10.2138/am-2000-8-901.

– (2006). *Quantitative Textural Measurements in Igneous and Metamorphic Petrology*. Cambridge University Press. ISBN: 9780521135153. DOI: 10.1017/cbo9780511535574.

Hill, R. E. T. (2001). "Komatiite volcanology, volcanological setting and primary geochemical properties of komatiite-associated nickel deposits". *Geochemistry: Exploration, Environment, Analysis* 1(4), pages 365–381. ISSN: 2041-4943. DOI: 10.1144/geochem.1.4.365.

Holness, M. B., R. Farr, and J. A. Neufeld (2017). "Crystal settling and convection in the Shiant Isles Main Sill". *Contributions to Mineralogy and Petrology* 172(1). ISSN: 1432-0967. DOI: 10.1007/s00410-016-1325-x.

Holness, M. B., Z. Vukmanovic, and B. O'Driscoll (2022). "The Formation of Chromite Chains and Clusters in Igneous Rocks". *Journal of Petrology* 64(1). ISSN: 1460-2415. DOI: 10.1093/petrology/egac124.

Hon, K., J. Kauahikaua, R. Denlinger, and K. MacKay (1994). "Emplacement and inflation of pahoehoe sheet flows: Observations and measurements of active lava flows on Kilauea Volcano, Hawaii". *Geological Society of America Bulletin* 106(3), pages 351–370. ISSN: 0016-7606. DOI: 10.1130/0016-7606(1994)106<0351:eaiops>2.3.co;2.

Jerram, D. A. and M. D. Higgins (2007). "3D Analysis of Rock Textures: Quantifying Igneous Microstructures". *Elements* 3(4), pages 239–245. ISSN: 1811-5217. DOI: 10.2113/gselements.3.4.239.

Kauahikaua, J., K. V. Cashman, T. N. Mattox, C. C. Heliker, K. A. Hon, M. T. Mangan, and C. R. Thornber (1998). "Observations on basaltic lava streams in tubes from Kilauea Volcano, island of Hawai'i". *Journal of Geophysical Research: Solid Earth* 103(B11), pages 27303–27323. ISSN: 0148-0227. DOI: 10.1029/97jb03576.

Kerr, R. C. and J. R. Lister (1991). "The Effects of Shape on Crystal Settling and on the Rheology of Magmas". *The Journal of Geology* 99(3), pages 457–467. ISSN: 1537-5269. DOI: 10.1086/629506.

Keszthelyi, L., A. S. McEwen, and T. Thordarson (2000). "Terrestrial analogs and thermal models for Martian flood lavas". *Journal of Geophysical Research: Planets* 105(E6), pages 15027–15049. ISSN: 0148-0227. DOI: 10.1029/1999je001191.

Latypov, R., S. Chistyakova, S. J. Barnes, B. Godel, G. W. Delaney, P. W. Cleary, V. J. Radermacher, I. Campbell, and K. Jakata (2022). "Chromitite layers indicate the existence of large, long-lived, and entirely molten magma chambers". *Scientific Reports* 12(1). ISSN: 2045-2322. DOI: 10.1038/s41598-022-08110-6.

Lockwood, J. and P. Lipman (1987). "Holocene eruptive history of Mauna Loa Volcano, Hawaii". *U.S. Geological Survey Professional Paper* 1350, pages 509–535.

Marsh, B. D. (1988). "Crystal size distribution (CSD) in rocks and the kinetics and dynamics of crystallization: I. Theory". *Contributions to Mineralogy and Petrology* 99(3), pages 277–291. ISSN: 1432-0967. DOI: 10.1007/bf00375362.

– (1998). "On the Interpretation of Crystal Size Distributions in Magmatic Systems". *Journal of Petrology* 39(4), pages 553–599. ISSN: 1460-2415. DOI: 10.1093/petroj/39.4.553.

– (2015). "Magma Chambers". *The Encyclopedia of Volcanoes*. Elsevier, pages 185–201. DOI: 10.1016/b978-0-12-385938-9.00008-0.

Mattox, T. N., C. Heliker, J. Kauahikaua, and K. Hon (1993). "Development of the 1990 Kalapana Flow Field, Kilauea Volcano, Hawaii". *Bulletin of Volcanology* 55(6), pages 407–413. ISSN: 1432-0819. DOI: 10.1007/bf00302000.

McIntire, M. Z., G. W. Bergantz, and J. M. Schleicher (2019). "On the hydrodynamics of crystal clustering". *Philosophical Transactions of the Royal Society A: Mathematical, Physical and Engineering Sciences* 377(2139), page 20180015. ISSN: 1471-2962. DOI: 10.1098/rsta.2018.0015.

Moore, H. (1987). "Preliminary estimates of the rheological properties of 1984 Mauna Loa lava". *U.S. Geological Survey Professional Paper* 1350, pages 1569–1588.

Perring, C., S. Barnes, M. Verrall, and R. Hill (2004). "Using automated digital image analysis to provide quantitative petrographic data on olivine–phyric basalts". *Computers & Geosciences* 30(2), pages 183–195. ISSN: 0098-3004. DOI: 10.1016/j.cageo.2003.10.005.

Philpotts, A. R. and L. D. Dickson (2000). "The formation of plagioclase chains during convective transfer in basaltic magma". *Nature* 406(6791), pages 59–61. ISSN: 1476-4687. DOI: 10.1038/35017542.

Rowland, S. K. and G. P. Walker (1988). "Mafic-crystal distributions, viscosities, and lava structures of some Hawaiian lava flows". *Journal of Volcanology and Geothermal Research* 35(1–2), pages 55–66. ISSN: 0377-0273. DOI: 10.1016/0377-0273(88)90005-4.

Ryan, C. G., D. P. Siddons, R. Kirkham, Z. Y. Li, M. D. de Jonge, D. J. Paterson, A. Kuczewski, D. L. Howard, P. A. Dunn, G. Falkenberg, U. Boesenberg, G. De Geronimo, L. A. Fisher, A. Halfpenny, M. J. Lintern, E. Lombi, K. A. Dyl, M. Jensen, G. F. Moorhead, J. S. Cleverley, R. M. Hough, B. Godel, S. J. Barnes, S. A. James, K. M. Spiers, M. Alfeld, G. Wellenreuther, Z. Vukmanovic, and S. Borg (2014). "Maia X-ray fluorescence imaging: Capturing detail in complex natural samples". *Journal of Physics: Conference Series* 499, page 012002. ISSN: 1742-6596. DOI: 10.1088/1742-6596/499/1/012002.

Schwindinger, K. R. and A. T. Anderson (1989). "Synneusis of Kilauea Iki olivines". *Contributions to Mineralogy and Petrology* 103(2), pages 187–198. ISSN: 1432-0967. DOI: 10.1007/bf00378504.

Self, S., T. Thordarson, L. Keszthelyi, G. P. L. Walker, K. Hon, M. T. Murphy, P. Long, and S. Finnemore (1996). "A new model for the emplacement of Columbia River basalts as large, inflated Pahoehoe Lava Flow Fields". *Geophysical Research Letters* 23(19), pages 2689–2692. DOI: https://doi.org/10.1029/96GL02450.

Self, S., T. Thordarson, and L. Keszthelyi (1997). "Emplacement of continental flood basalt lava flows". *Geophysical Monograph Series* 100, pages 381–410. DOI: 10.1029/GM100p0381.

Sherrod, D. R., J. M. Sinton, S. E. Watkins, and K. M. Brunt (2021). *Geologic map of the State of Hawaii*. DOI: 10.3133/sim3143.

Smith, R. E. (1967). "Segregation vesicles in basaltic lava". *American Journal of Science* 265(8), pages 696–713. ISSN: 0002-9599. DOI: 10.2475/ajs.265.8.696.

Thordarson, T. and S. Self (1996). "Morphology and structures of pahoehoe sheet flow units: Examples from flood lavas in Iceland and Columbia River Basalt Group". Edited by P. W. Whitehead. James Cook University of Northern Queensland, Townsville, pages 90–91.

– (1998). "The Roza Member, Columbia River Basalt Group: A gigantic pahoehoe lava flow field formed by endogenous processes?" *Journal of Geophysical Research: Solid Earth* 103(B11), pages 27411–27445. ISSN: 0148-0227. DOI: 10.1029/98jb01355.

Trusdell, F. A. and J. P. Lockwood (2017). *Geologic map of the northeast flank of Mauna Loa volcano, Island of Hawai'i, Hawaii*. DOI: 10.3133/sim2932a.

Ubide, T. and B. S. Kamber (2018). "Volcanic crystals as time capsules of eruption history". *Nature Communications* 9(1). ISSN: 2041-1723. DOI: 10.1038/s41467-017-02274-w.

Vance, J. A. (1969). "On synneusis". *Contributions to Mineralogy and Petrology* 24(1), pages 7–29. ISSN: 1432-0967. DOI: 10.1007/bf00398750.

Walker, G. P. L. (1971). "Compound and simple lava flows and flood basalts". *Bulletin Volcanologique* 35(3), pages 579–590. ISSN: 1432-0819. DOI: 10.1007/bf02596829.

Welsch, B., F. Faure, V. Famin, A. Baronnet, and P. Bachèlery (2013). "Dendritic Crystallization: A Single Process for all the Textures of Olivine in Basalts?" *Journal of Petrology* 54(3), pages 539–574. ISSN: 0022-3530. DOI: 10.1093/petrology/egs077.

Wieser, P. E., Z. Vukmanovic, R. Kilian, E. Ringe, M. B. Holness, J. Maclennan, and M. Edmonds (2019). "To sink, swim, twin, or nucleate: A critical appraisal of crystal aggregation processes". *Geology* 47(10), pages 948–952. ISSN: 1943-2682. DOI: 10.1130/g46660.1.